Parameter Estimation and Indirect Vector Control of AC Induction Motor

A THESIS
SUBMITTED TO THE FACULTY OF GRADUATE SCHOOL
OF THE UNIVERSITY OF MINNESOTA
BY

Lakshmi Narayanan Srivatchan

IN PARTIAL FULFILLMENT OF THE REQUIREMENTS
FOR THE DEGREE OF
MASTER SCIENCE

Advisor: Professor Ned Mohan

January, 2014

Acknowledgements

I would like to express my deepest gratitude and sincere thanks to my advisor Professor Ned Mohan for his continued support, guidance and patience during my graduate studies at the University of Minnesota. His mentorship as a leading researcher and thoughtful advisor has helped me become an independent thinker and shape my goals in life. I would also like to thank Professor Peter Seiler for his guidance through courses in the field of control systems which has inspired an area of research interest within me. I would also like to convey my thankfulness to Professor Bruce F. Wollenberg for his enthusiasm towards this project.

I would like to specially thank Siddharth Raju as a colleague and childhood friend for supporting me through moments of despair. His contribution towards my personal and academic growth is immense and has made my journey as a graduate student pleasurable. I would also like to thank all members of Prof. Ned Mohan's research group for their ideas with this project.

I would like to thank Linestream Technologies for inspiring new ideas and extending the scope of this research topic.

Finally, I owe it to my family for their constant backing towards all my endeavors in life. Their advice during moments of difficulties has helped me stay on the right path and be a successful human being.

Dedication

To My Family.

Abstract

Industrial motor drive applications are usually complex and expensive. Most industries invest time and effort to implement drives which are low-cost, reliable, energy efficient and require low maintenance. In this field, the Induction motor (IM) is popular for its superior performance compared to its counterparts. There are two types of IM- squirrel cage IM and wound rotor IM both widely used. The popularity of the squirrel cage induction machine is attributed to its ruggedness (high output power to size ratio) and simplicity of construction. Recent advances in power electronics such as the Voltage Source Inverter (VSI) based drives have enabled variable speed control of IM's. VSI based drive converts DC voltage into three phase voltage of variable magnitude and frequency based on requirements for motor control. Well established knowledge in the fields of Digital Signal Processing (DSP), high performance microcontrollers, and analog sensors has aided the growth of motor controllers.

This thesis has its foundation on a certain form of control called Indirect Vector control based on frame transformations, estimators and error based controllers. Chapter 1 discusses the basics of frame transformations, its advantages and modeling the IM in a new frame called the *dq*-frame. Chapter 2 examines the indirect vector control on the *dq*- frame and lays the foundation for simulation study. Chapter 3 deals with the method used to arrive at motor parameters and discusses the importance of accuracy of these values. It also expands on the vector control foundation by building a mathematical model of some of the components of the control used for simulation studies. Chapter 4 discusses in detail the design of error based controllers and presents a simple comparative study between different controllers. Chapter 5 talks about the simulation and hardware setup and provides the respective results.

Table of Contents

List of Tables

List of Figures

Chapter 1

dq –Theory for Induction Machine

1.1 Introduction

In any 3-phase system there are three control parameters- voltage magnitude, phase angle and frequency. In an IM the three phase stator windings are separated by 120 degrees. To ensure uniform flux distribution in the air-gap, the stator currents must be equal in magnitude and have a phase shift of 120 degrees to each other. Any deviation from this would lead to non-uniform flux distribution which causes harmonic oscillations in the electromechanical torque. This has been a reason for many motor failures typically characterized by breaking of the shaft. This leads to two available control variables – the input voltage magnitude and frequency.

This chapter aims at building a transformation theory aiming to bring a direct correlation between the control parameters - torque and flux and the controllable parameters- voltage magnitude and frequency. An IM is a 3-phase 3-wire system where the neutral is not accessible. This leads to the fact that sum of any three phase variables is always zero. This constraint has been used to transform the three phase linearly dependent quantities to two phase linearly independent quantities (1).

1.2 3-phase to 2-phase transformation

In the past various control techniques without the use of transformations have been employed, the most popular being volts-per-hertz (v/f) control as shown in (2). These techniques show poor performance in comparison to vector control technique due to lack of direct explicit relationship between the controlled parameters and controllable parameters.

The Clark's$\alpha\beta$ transformation transforms the three phase sinusoidal quantities into two phase sinusoidal quantities. We will see that this transformation helps bring about a direct relationship between the controllable and the control parameters. Equation (1-1) shows Clark's transform. If the input *abc*-signals are sinusoidally varying this result in sinusoidally varying $\alpha\beta$ quantities as seen in equations (1-2), (1-3) and (1-4).

$$\begin{bmatrix} u_\alpha \\ u_\beta \\ u_0 \end{bmatrix} = \begin{bmatrix} \frac{2}{3} & -\frac{1}{3} & -\frac{1}{3} \\ 0 & \frac{1}{\sqrt{3}} & \frac{1}{\sqrt{3}} \\ \frac{1}{3} & \frac{1}{3} & \frac{1}{3} \end{bmatrix} \begin{bmatrix} u_a \\ u_b \\ u_c \end{bmatrix} \quad (1\text{-}1)$$

$$\begin{bmatrix} u_\alpha \\ u_\beta \\ u_0 \end{bmatrix} = \begin{bmatrix} \frac{2}{3} & -\frac{1}{3} & -\frac{1}{3} \\ 0 & \frac{1}{\sqrt{3}} & \frac{1}{\sqrt{3}} \\ \frac{1}{3} & \frac{1}{3} & \frac{1}{3} \end{bmatrix} \begin{bmatrix} u\,sin(\omega t) \\ u\,sin(\omega t - 120) \\ u\,sin(\omega t - 240) \end{bmatrix} \quad (1\text{-}2)$$

$$u_\alpha = u\,sin(\omega t) \quad (1\text{-}3)$$

$$u_\beta = -\frac{1}{\sqrt{3}} u \sin(\omega t) \quad (1\text{-}4)$$

The control technique using Clark's $\alpha\beta$ transformation is complicated due to sinusoidally varying nature of the signals as shown above. The *abc* to *dq* transformation or the Park's transform transforms the sinusoidally varying quantities into dc quantities. This is achieved by rotating the $\alpha\beta$ plane at a speed ω_d as given by equation (1-5). The quantity u_0 becomes zero in the case of three phase three wire systems.

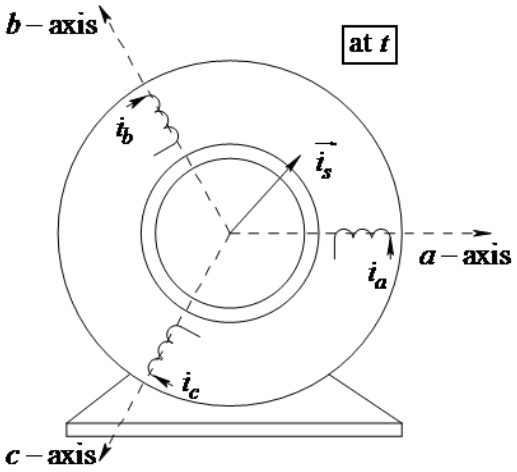

Figure 1-2 Three phase stator current representation (Advanced Electric Drives by Ned Mohan, 2001: p.3-2)

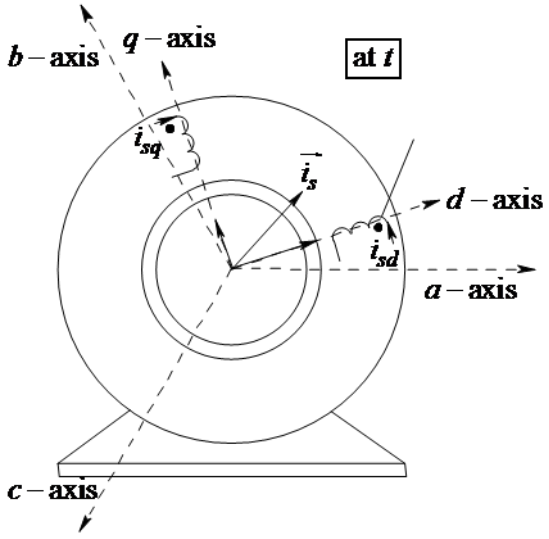

Figure 1-1 dq representation of stator currents (Advanced Electric Drives by Ned Mohan, 2001: p.3-2)

$$\begin{bmatrix} u_d \\ u_q \\ u_0 \end{bmatrix} = \sqrt{\frac{2}{3}} \begin{bmatrix} \cos(\omega_d t) & \cos(\omega_d t - \frac{2\pi}{3}) & \cos(\omega_d t - \frac{4\pi}{3}) \\ -\sin(\omega_d t) & -\sin(\omega_d t - \frac{2\pi}{3}) & -\sin(\omega_d t - \frac{4\pi}{3}) \\ 1 & 1 & 1 \end{bmatrix} \begin{bmatrix} u_a \\ u_b \\ u_c \end{bmatrix} \quad (1\text{-}5)$$

1.3 Induction motor *dq* model

Using Park's transformation the three phase stator (*abc*) winding shown in Figure 1-2 can be equivalently seen as synchronously rotating two phase (*dq*) quadrature winding as shown in Figure 1-1

Since the *d* and the *q* axis windings are at 90° to each other there is no mutual coupling between them. We have four set of *dq* windings – the stator *d* and *q* axis winding and the rotor *d* and *q* axis winding as shown in Figure 1-3. The stator *d* axis flux linkage $\lambda_{sd}$is produced by the combined contribution of the stator *d* axis current i_{sd} and its associated stator inductance L_s and the rotor *d* axis current i_{rd} and the magnetizing inductance L_m. Expressions for $\lambda_{sq}\lambda_{rd}$ and λ_{rq} are derived as shown in equations (1-6), (1-7), (1-8) and (1-9).

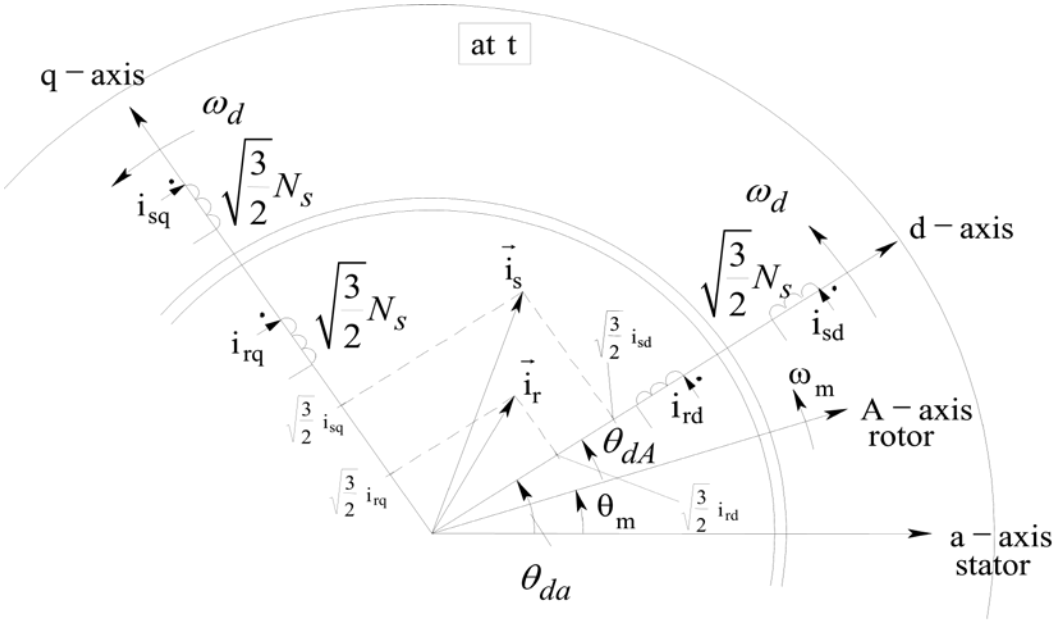

Figure 1-3 Stator and rotor representation by equivalent dq winding currents. (Advanced Electric Drives by Ned Mohan, 2001: p.3-6)

$$\lambda_{sd} = L_s i_{sd} + L_m i_{rd} \quad (1\text{-}6)$$

$$\lambda_{sq} = L_s i_{sq} + L_m i_{rq} \quad (1\text{-}7)$$

$$\lambda_{rd} = L_r i_{rd} + L_m i_{sd} \quad (1\text{-}8)$$

$$\lambda_{rq} = L_r i_{rq} + L_m i_{sq} \quad (1\text{-}9)$$

In order to derive the *dq*-winding voltage dynamic equation we transform three phase *abc* quantities into two phase stationary $\alpha\beta$quantities as shown in Figure 1-4. Once we have the voltage dynamic equation in the $\alpha\beta$ coordinates these quantities are re-written in the *dq* frame having $\alpha\beta$ reference to obtain the dynamic equations in *dq* reference frame. The stator and the rotor *dq* voltages are derived in (3) and presented in equations (1-10), (1-11) and(1-12), (1-13).

$$v_{sd} = R_s i_{sd} + \frac{d}{dt}\lambda_{sd} - \omega_d \lambda_{sq} \quad (1\text{-}10)$$

$$v_{sq} = R_s i_{sq} + \frac{d}{dt}\lambda_{sq} + \omega_d \lambda_{sd} \quad (1\text{-}11)$$

$$v_{rd} = R_r i_{rd} + \frac{d}{dt}\lambda_{rd} - \omega_{dA} \lambda_{rq} \quad (1\text{-}12)$$

$$v_{rq} = R_r i_{rq} + \frac{d}{dt}\lambda_{rq} + \omega_{dA} \lambda_{rd} \quad (1\text{-}13)$$

$$\omega_d = \frac{d}{dt}\theta_{da} \quad (1\text{-}14)$$

$$\omega_{dA} = \frac{d}{dt}\theta_{dA} \quad (1\text{-}15)$$

In equation (1-10) and (1-11) ω_d is the instantaneous speed of the *dq* winding set in the air gap as shown in Figure 1-4 and is obtained by differentiating the *d*-axis orientation with respect to the stationary *a* axis as shown in equation (1-14). Similarly ω_{dA} is the instantaneous speed of the dq winding with respect to rotor *A* axis winding as shown in equation (1-15) where θ_{dA} is the orientation of the *d*-axis with respect to the rotating rotor *A* axis winding. The net electromagnetic torque is derived in (3) and is presented in equation (1-16).

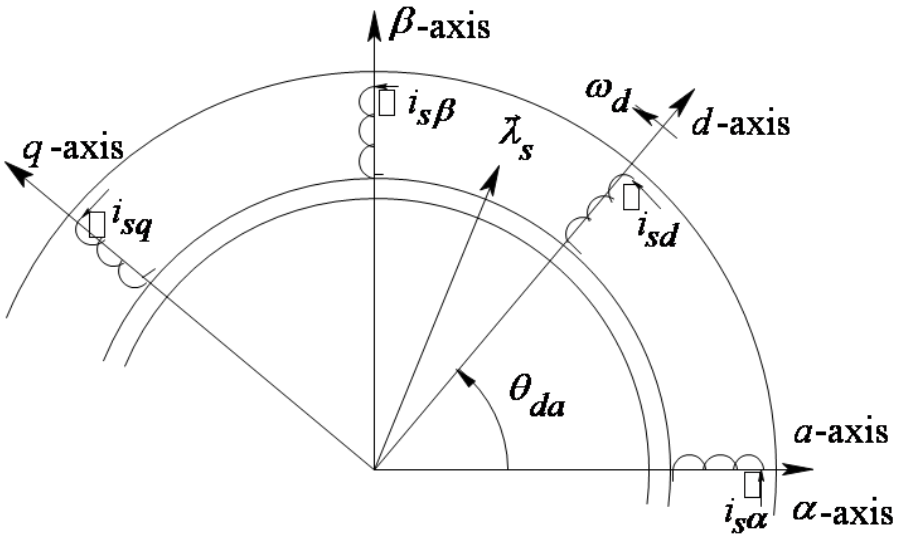

Figure 1-4 Stator alpha-beta and dq winding representation (Advanced Electric Drives by Ned Mohan, 2001: p.3-11)

Substituting for flux-linkage quantities in equations (1-10) through (1-13) in terms of inductances from equation (1-6) through (1-9) for the stator and rotor quantities we get the following expanded *dq*-winding voltage equations as shown in equations (1-17), (1-18), (1-19) and (1-20).Using these equations, the *dq* model of the induction motor is constructed and is shown in Figure 1-5.

$$T_{em} = \frac{p}{2} L_m (i_{sq} i_{rd} - i_{sd} i_{rq}) \quad (1\text{-}16)$$

$$v_{sd} = R_s i_{sd} - \omega_d \lambda_{sq} + L_{ls} \frac{d}{dt} i_{sd} + L_m \frac{d}{dt} (i_{sd} + i_{rd}) \quad (1\text{-}17)$$

$$v_{sq} = R_s i_{sq} + \omega_d \lambda_{sd} + L_{ls} \frac{d}{dt} i_{sq} + L_m \frac{d}{dt} (i_{sq} + i_{rq}) \quad (1\text{-}18)$$

$$v_{rd} = R_r i_{rd} - \omega_{dA} \lambda_{rq} + L_{lr} \frac{d}{dt} i_{rd} + L_m \frac{d}{dt} (i_{sd} + i_{rd}) \quad (1\text{-}19)$$

$$v_{rq} = R_r i_{rq} + \omega_{dA} \lambda_{rd} + L_{lr} \frac{d}{dt} i_{rq} + L_m \frac{d}{dt} (i_{sq} + i_{rq}) \quad (1\text{-}20)$$

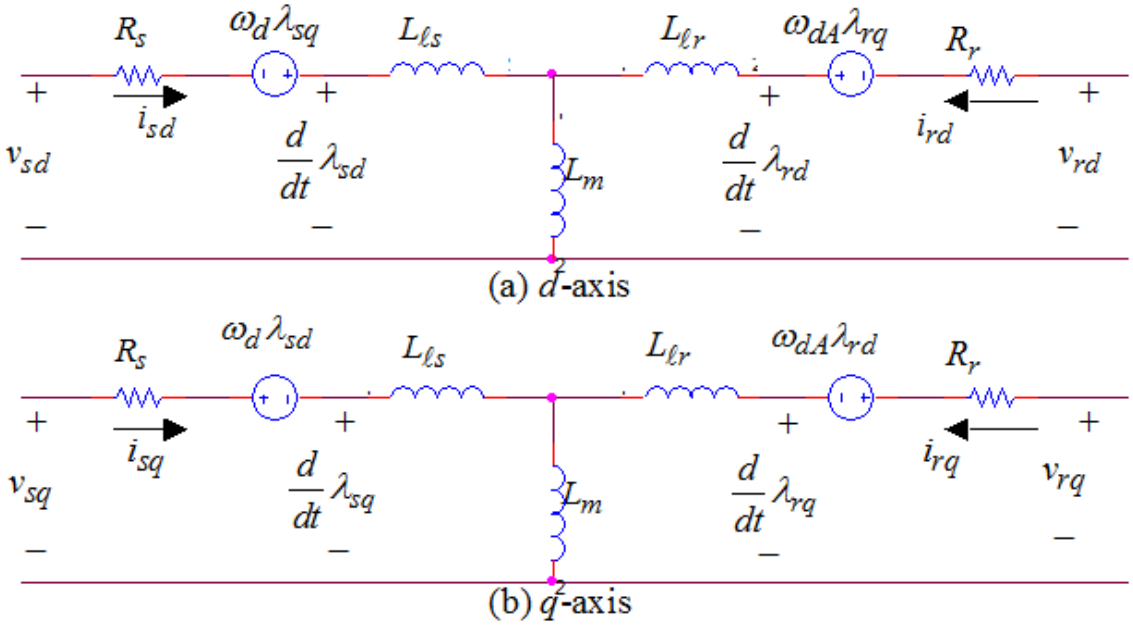

Figure 1-5 *dq* winding equivalent circuit (Advanced Electric Drives by Ned Mohan, 2001: p.3-21)

1.4 Conclusion

In this chapter, the mathematical transformation that converts a three axis system into two axis system was discussed. Using this transformation technique as the foundation, a mathematical model of the IM in the two axis *dq* model of the IM was derived. There are many merits to

transforming the three axis IM model into two axis system such as no magnetic coupling between the *d* and *q* axis due to their perpendicular orientation to each other. This transformation technique when applied to the IM leads to simple expression for electromagnetic torque and rotor flux which can be controlled independently. This is discussed in greater detail in the following chapter through a mathematical discussion.

Chapter 2

Vector control of Induction motor

2.1 Introduction

The concept of vector control of Induction motor first came about in the 1970's and has ever since revolutionized control of ac drives. Though traditional methods of control such as v/f control satisfied objectives, the v/f control has poor performance to fast changing signals (2). In vector control of IM good performance is ensured by employing transformation techniques which uncouples inter-dependant quantities. This enables the IM to be controlled using independent signals that exclusively controls the control variables.

In vector control, the induction machine quantities appear as dc signals in the rotating *dq* frame. The stator d-axis current, i_{sd} is used to control the rotor flux and stator q-axis current, i_{sq} is used to control the torque. This ensures independent control of torque and flux in the machine which are naturally orthogonal to each other in steady state.Since these signals are dc in the rotating *dq* frame it makes for easy control using proportional integral (PI) controllers.

Accurate vector control involves good control of the stator d and q-axis currents and accurate estimation of rotor flux position. The rotor flux position allows transformation of quantities from the rotating reference frame to the stationary reference frame. Based on the method used to estimate rotor flux position, vector control is classified into direct and indirect vector control as per (4).

2.2 Indirect Vector Control of Induction motor

In indirect vector control the rotor flux position is estimated indirectly using estimates of the rotor flux and stator q-axis current. In the following control scheme, the d-axis is aligned with the rotor flux linkage space vector $\overrightarrow{\lambda_r}$ as shown in Figure 2-1.

2.2.1 q-axis Rotor Dynamics

Aligning the rotor flux linkage space vector $\overrightarrow{\lambda_r}$ along the d-axis leads to $\lambda_{rq} = 0$ and substituting this condition in equation (1-9) gives us equation (2-1). It is necessary to produce a step change in rotor q-axis current in order to produce a step change in torque in the machine. This is apparent by observing the striking similarity between equation (2-1) and a transformer's winding currents. In fact, the behavior of the induction machine in vector control along the q-axis is very similar to the behavior of a transformer.

$$i_{rq} = -\frac{L_m}{L_r} i_{sq} \qquad (2\text{-}1)$$

2.2.1.1 Transformer analogy with q-Axis Rotor Dynamics

Consider a simple transformer. For ease of understanding, let us call the primary of the transformer as the stator (suffix s) and secondary as the rotor (suffix r). Since stator currents are used as controllable parameters in vector control, let us consider the stator to be excited by an independent current source. The equations governing the transformer flux linkages are written below.

$$\lambda_s = L_s i_s + L_m i_r \qquad (2\text{-}2)$$

$$\lambda_r = L_r i_r + L_m i_s \quad (2\text{-}3)$$

$$\frac{d}{dt}\lambda_r = -R_r i_r \quad (2\text{-}4)$$

$$i_r(s) = -\frac{sL_m}{R_r + sL_r} i_s(s) \quad (2\text{-}5)$$

$$\lambda_r(s) = \frac{L_m R_r}{R_r + sL_r} i_s(s) \quad (2\text{-}6)$$

Let us now consider a step change in stator current. In order to produce a step change in current in the presence of leakage fluxes, a voltage impulse is required which is explained in (3). From equation (2-7) we see that a step change in primary current at t=0+ is accompanied by a negative step in rotor current. Notice that this equation matches with equation (2-1) derived from the *dq*-model of Induction motor for the vector control. However, this does not change the rotor flux linkage λ_r because the sudden appearance of flux linkage $L_m i_s$ is countered by a self-flux linkage $L_r i_r$. This is the essence of q-axis dynamics in vector control where a step change in stator q-axis current produces a step change in rotor q-axis current without changing the flux linkage along the q-axis at that instant of time.

$$i_r = -\frac{L_m}{L_r} i_s att = 0^+ \quad (2\text{-}7)$$

For t>0+ the transformer rotor current and flux linkage adjust to a value based on the time constant of the rotor circuit. The transformer rotor current would decay to zero which would result in no torque. To overcome the decay of induction motor q-axis rotor current, it is necessary to rotate the d and q axis at a certain speed.

2.2.2 Calculation of *dq*-axis speed ω_{dA}

With d-axis aligned with rotor flux$d\ \lambda_{rq}/dt = 0$. Substituting this condition into equation (1-13) of *dq*-model of IM gives us equation (2-8) where τ_r is the rotor time constant given by equation (2-9).

$$\omega_{dA} = \frac{L_m}{\tau_r \lambda_{rd}} i_{sq} \quad (2\text{-}8)$$

$$\tau_r = \frac{L_r}{R_r} \quad (2\text{-}9)$$

To get a better insight into the above expressions, consider an IM with its rotor blocked from turning as shown in Figure 2-1. At t=0+ a step change in i_{sq} prompts a step change in i_{rq} as argued in the previous section. However, the rotor currents decay for t> 0+. To prevent this, the d-axis and q-axis stator windings are rotated at an appropriate speed ω_{slip} so that $\overrightarrow{\lambda_r}$ is oriented along the d-axis at all time. Since the rotor flux linkage is always aligned with the d-axis and is a constant, the λ_r induces a voltage in the rotor bars which counteracts the iR_{bar} voltage drop. Hence, this voltage injection in the rotor circuit by rotating the d-axis and q-axis at ω_{slip} with locked rotor prevents decaying of currents in the rotor circuit and enables a constant rotor current necessary for producing a constant torque.

2.2.3 Calculation of Electromagnetic Torque

From the *dq*-model for induction motor, it can be shown from (3) that the electro-magnetic torque is related to the rotor and stator flux linkage and currents according to equation (1-16). Substituting $\lambda_{rq} = 0$ in the above expression we get equation (2-10). The electromagnetic torque depends on the stator q-axis current and rotor flux linkage vector aligned along the d-axis.

$$T_{em} = -\frac{p}{2}\frac{L_m}{L_r} i_{sq} \lambda_{rd} \quad (2\text{-}10)$$

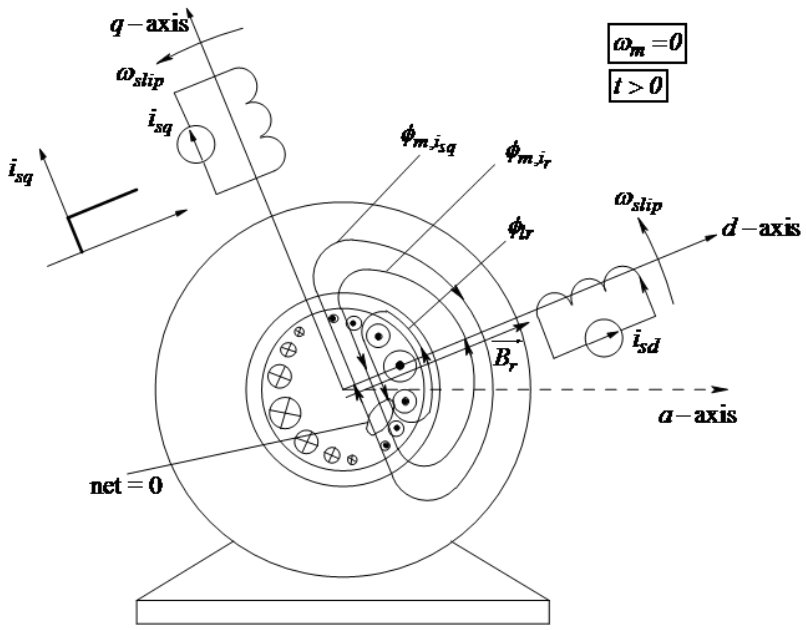

Figure 2-1 Current and fluxes in machine with rotor blocked(Advanced Electric Drives by Ned Mohan, 2001: p.4-14)

2.2.4 Flux Linkage Dynamics along Rotor d-Axis

Consider the equivalent circuit shown in Figure 2-2 obtained from the induction motor *dq*-model. Equation (2-11) relates the stator d-axis current and rotor flux linkage space vector along the d-axis. Prior to t=0- the magnetizing currents along the three phases are built up such that $i_{sd}(0^-)$ produces the rated magnetic flux in the machine. Once this flux is built-up, the machine can be commanded any reference speed signals for tracking.

$$\frac{d}{dt}\lambda_{rd} + \frac{\lambda_{rd}}{\tau_r} = \frac{L_m}{\tau_r} i_{sd} \quad (2\text{-}11)$$

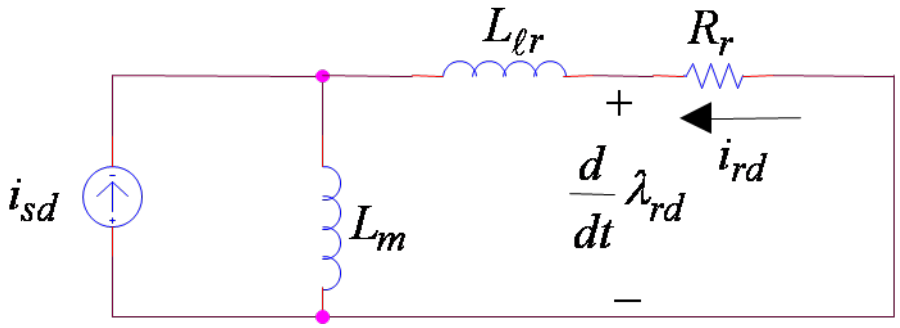

Figure 2-2 d-axis rotor dynamics circuit representation (Advanced Electric Drives by Ned Mohan, 2001: p.5-5)

2.2.5 Estimation of Rotor Flux orientation θ_{da}

From equation (2-8) we have a mathematical way of estimating the d-axis speed with respect to the rotor A-axis. Since the rotor flux is aligned to the d-axis, ω_{dA} measures the rotor flux speed with respect to the rotor A-axis. Using the data provided by the position sensor, the mechanical speed of the motorω_m is available. From a stationary frame equation (2-12) provides the speed of the d-axis with respect to the stationary a-axis. Integrating equation (2-12) gives us equation (2-13)which is the orientation of rotor flux with respect to the stationary-a axis.

$$\omega_d = \omega_m + \omega_{dA} \qquad (2\text{-}12)$$

$$\theta_{da} = \int_0^t \omega_{da}(\tau)d\tau \qquad (2\text{-}13)$$

2.3 Conclusion:

In this chapter, we developed a model of the Induction motor with d-axis aligned to the rotor flux linkage space vector. We derived empirical equations under this alignment conditions and showed how the various parameters can be controlled from the stator side. This chapter serves as the foundation to the mathematical model discussed on Chapter 3 and the results presented in Chapter 5. We notice that the mathematical equations derived in this chapter are heavily dependent on the electrical and mechanical parameters. The first part of Chapter 3 discusses the methodology used in arriving at these parameters and the various factors to take into consideration for the same.

Chapter 3

Parameter Estimation and Mathematical Modeling

3.1 Introduction

The major aspect of precise position, velocity and torque control is the accurate estimation of motor parameters. Even a very small variation in these parameters could lead to drastic changes in the output performance (5). The motor parameters such as turns ratio and number of poles are constant while parameters such as winding resistance and magnetizing inductance can be estimated only with a certain degree of precision. These parameters can be measured directly or can be estimated by simple calculations. These parameters vary depending on the temperature and magnetic flux density. The parameters such as rotor and stator leakage inductances require complex modeling and numerical simulations and hence only an approximate estimate of these quantities is available. Motor parameters such as load inertia vary dynamically. The control loops are hence designed for the most optimal load values.

3.2 Parameter Estimation

Under steady state the electrical side of an induction motor can be seen as a transformer. The per-phase steady state equivalent circuit of an induction motor is shown in Figure 3-1.

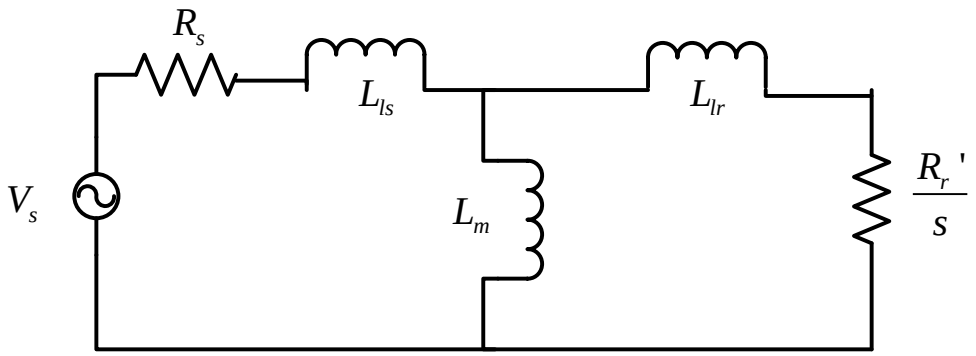

Figure 3-1Per phase representation of IM (Electric Drives by Ned Mohan, 2003: p.11-28)

3.2.1 Stator resistance R_s

3.2.1.1 Determination of stator resistanceR_s

The stator resistance can be estimated by DC measurement of the stator resistance of any two phases as per equation (3-1) using a mutlimeter.

$$R_s = R_{phase-phase}/2 \quad (3\text{-}1)$$

3.2.1.2 Variation of Stator resistance R_s

Although this estimation of stator resistance is sufficient for designing a controller, this is an inaccurate measure since the multimeter lead resistance gets added to the stator resistance measure. The value of the stator resistance varies with changes in frequency due to skin effect and the temperature which could be accounted to provide a more accurate measure (6).

3.2.2 Magnetizing inductance L_m

3.2.2.1 Determination of magnetizing inductance L_m

In order to determine the magnetizing inductance of the induction motor it is coupled with a DC motor which is run under speed control at the rated mechanical synchronous speed. This sets the coupled induction motor to rotate at the rated mechanical synchronous speed which is also supplied the rated frequency at its input. In this condition the induction motor is having zero slip and leads to the rotor circuit being open circuited. The following quantities are measured; the per phase rms voltage V_{arms} ($V_{ll}/\sqrt{3}$), the per phase rms current I_{arms} and the phase angle (θ) difference between the phase voltage and current. Since the leakage inductance is extremely small compared to the magnetizing inductance, it is assumed that the entire reactive power is stored in the magnetizing inductance. The magnetizing inductance and reactance is calculated based on the reactive power stored in the magnetizing inductance as per equation (3-2). The reactive power is used to calculate the magnetizing inductance as per equation (3-3).

$$Q = V_{arms} I_{arms} \sin\theta \quad (3\text{-}2)$$

$$L_m = \frac{Q}{2\pi f_{sync} {I_{arms}}^2} \quad (3\text{-}3)$$

3.2.2.2 Variation of magnetizing inductance L_m

Having an accurate value of magnetizing inductance is of most importance to ensure efficient control of IM. This is because L_m influences the estimation of rotor flux density B_r and the rotor currentI_r, both of which contribute to controlling the torque in the IM. This method of estimating magnetizing inductance is very inaccurate as the influence of stator leakage inductance in the calculation is getting ignored. The magnetizing inductance varies by several tens of percentage

according to the excitation current. It is thus important to measure magnetizing inductance using rated value of current.

3.2.3 Rotor and Stator leakage inductances and rotor resistance L_{lr}, L_{ls} and R_r'

3.2.3.1 Determination of L_{lr}, L_{ls} and R_r'

To compute the rotor and stator leakage inductance and rotor resistance as seen from the stator, the induction machine is run under slip=1. Under this condition, the equivalent impedance seen by the machine terminals is as per equation (3-4). If we assume the condition shown in equation (3-5), back substituting into equation (3-4), R_r' can be computed as shown in (7).

$$Z_{machine} = j\omega(L_{lr} + L_{ls}) + R_r' + R_s \quad (3\text{-}4)$$

$$L_{ls} = \frac{2}{3} L_{lr} \quad (3\text{-}5)$$

In this determination, the induction motor is coupled with a DC motor. Firstly, the induction motor is supplied its rated frequency and the DC motor is run in torque control. The DC motor torque is increased until the induction motor draws its rated current and is operating at its rated conditions. The speed of the Induction motor ω_m is noted so that the slip speed can be determined as per equations (3-6) and (3-7).

$$\omega_{slip} = \omega_{sync} - \omega_m \quad (3\text{-}6)$$

$$f_{slip} = \omega_{slip}/(2\pi) \quad (3\text{-}7)$$

After determining the slip frequency of the induction machine at rated conditions, the DC motor is run at speed control with a reference speed of zero RPM which represents a load. Now, the

induction motor is supplied a reference frequency of f_{slip} and the supply voltage is set such that the induction motor draws the rated current. Note down the peak voltage, current and the time difference between the voltage and current and follow equations (3-8) to (3-15) to compute L_{lr}, L_{ls} and R_r'.

$$I_{rms} = \hat{I}/\sqrt{2} \quad (3\text{-}8)$$

$$V_{rms} = \hat{V}/\sqrt{2} \quad (3\text{-}9)$$

$$\theta = \Delta t 2\pi f_{slip} \quad (3\text{-}10)$$

$$Z = \frac{V_{rms}}{I_{rms}}\hat{\theta} \quad (3\text{-}11)$$

$$L_{tot} = \frac{img(Z)}{2\pi f_{slip}} \quad (3\text{-}12)$$

$$L_{lr} = \frac{3}{5}L_{tot} \quad (3\text{-}13)$$

$$L_{ls} = \frac{2}{5}L_{tot} \quad (3\text{-}14)$$

$$R_r' = real(Z) - R_s \quad (3\text{-}15)$$

Equation (3-13) and (3-14) is a reasonable approximation because usually the slots in the stator are open compared to the closed slots in the rotor. Hence, the leakage inductance due to the magnetic saturation of the stator leakage flux is not severe compared to that of the rotor leakage inductance. This however varies based on the magnitude of the stator current.

3.2.3.2 Variation of rotor resistance R_r'

The rotor resistance varies according the slip frequency ω_{slip} in the rotor conductors. The rotor resistance varies by the skin effect which results in higher resistance as ω_{slip} increases. This

behavior can be used in obtaining a high starting torque without compromising on the efficiency. In addition to skin effect, the rotor resistance also varies with the temperature of the conductor and varies according to the temperature co-efficient of the rotor conductor material. These details need to be taken into considerations to operate the IM at the highest efficiency.

3.2.3.3 Variation of rotor leakage inductanceL_{lr}

The rotor leakage inductance, L_{lr} decreases as the slip frequency ω_{slip} increases due to skin effect. Magnetic saturation also affects the leakage flux in the rotor.

3.2.3.4 Variation of stator leakage inductanceL_{ls}

The stator leakage inductance varies due to the magnetic saturation of the stator core. It is therefore important to operate the IM in the linear region of the IM.

3.3 Mathematical Modeling

To predict and verify the performance of vector control strategy applied for induction motor, simulation study is carried out using MATLAB Simulink. The Simulink/MATLAB implementation is adopted because of its inherent advantages such as ease of implementation in block diagram form, various numerical solvers for complex computations and the flexibility to verify controller performance using other tool-box. The following section of this chapter initially provides an overview of the various components of vector control modeling and then provides an in-depth discussion into the mathematical modeling of the induction motor model, estimator model, load model and controller model.

3.3.1 Block diagram overview of Vector Control

Figure 3-2 shows the block diagram overview of the Induction motor vector control used for mathematical modeling and simulation studies. It can be seen that the mathematical model consists of the estimator block, the IM model, *dq* to *abc* block and the various controllers.

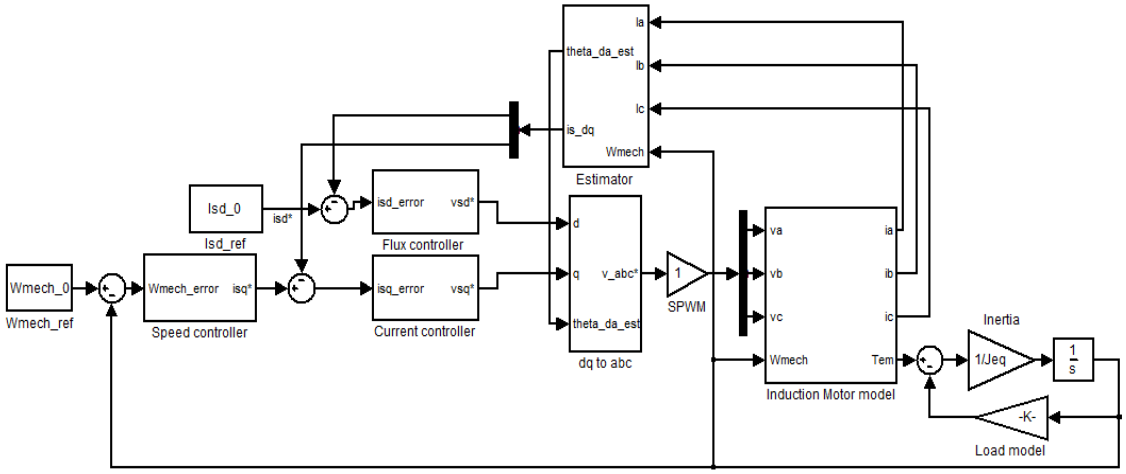

Figure 3-2 Block diagram overview of vector control of IM

3.3.2 Induction motor modeling

The *dq*-model of the induction motor discussed in Chapter-1 and is used instead of the usual *abc*-model as it reduces computational overhead. The dq stator and rotor voltage equations shown in equation (1-10) to (1-13) can be equivalently represented in matrix form as in equation (3-16) and (3-17). Similarly, equations (1-6) to (1-9) have been represented in equation (3-18). Re-writing expression for torque in equation (1-16) below in equation (3-19),the mathematical model representing the induction motor designed using MATLAB is shown in Figure 3-3.

$$\begin{bmatrix} v_{sd} \\ v_{sq} \end{bmatrix} = R_s \begin{bmatrix} i_{sd} \\ i_{sq} \end{bmatrix} + \frac{d}{dt} \begin{bmatrix} \lambda_{sd} \\ \lambda_{sq} \end{bmatrix} + \omega_d \begin{bmatrix} 0 & -1 \\ 1 & 0 \end{bmatrix} \begin{bmatrix} \lambda_{sd} \\ \lambda_{sq} \end{bmatrix} \quad (3\text{-}16)$$

$$\begin{bmatrix} v_{rd} \\ v_{rq} \end{bmatrix} = R_r \begin{bmatrix} i_{rd} \\ i_{rq} \end{bmatrix} + \frac{d}{dt} \begin{bmatrix} \lambda_{rd} \\ \lambda_{rq} \end{bmatrix} + \omega_{dA} \begin{bmatrix} 0 & -1 \\ 1 & 0 \end{bmatrix} \begin{bmatrix} \lambda_{rd} \\ \lambda_{rq} \end{bmatrix} \quad (3\text{-}17)$$

$$\begin{bmatrix} \lambda_{sd} \\ \lambda_{sq} \\ \lambda_{rd} \\ \lambda_{rq} \end{bmatrix} = \begin{bmatrix} L_s & 0 & L_m & 0 \\ 0 & L_s & 0 & L_m \\ L_m & 0 & L_r & 0 \\ 0 & L_m & 0 & L_r \end{bmatrix} \begin{bmatrix} i_{sd} \\ i_{sq} \\ i_{rd} \\ i_{rq} \end{bmatrix} \quad (3\text{-}18)$$

$$T_{em} = \frac{p}{2} L_m (i_{sq} i_{rd} - i_{sd} i_{rq}) \quad (3\text{-}19)$$

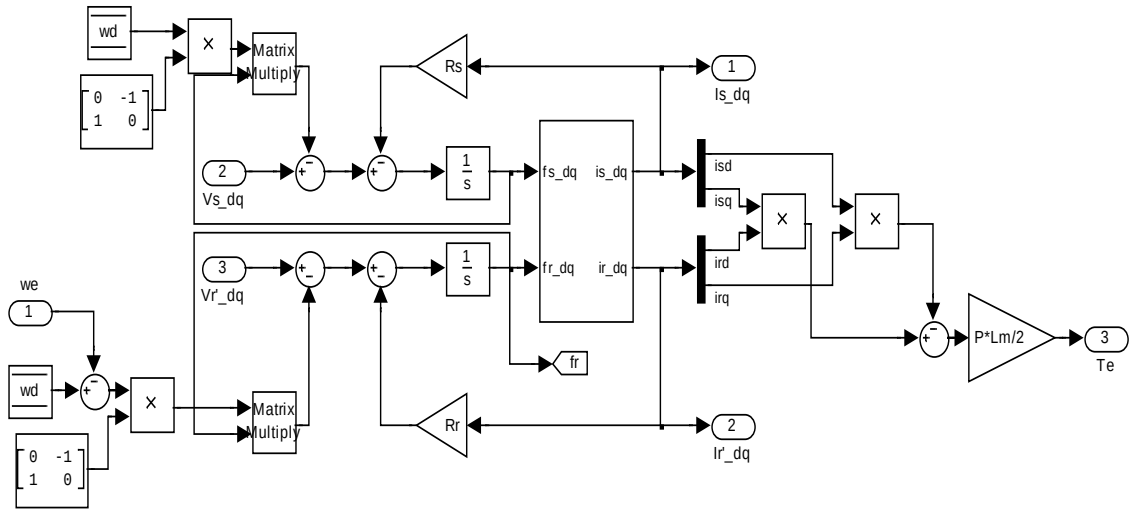

Figure 3-3 IM dq model block diagram

3.3.3 Estimator modeling

In vector control, the controller is designed to achieve reference speed and reference flux. The relationship between the speed, flux and *dq* currents is obtained with the assumption that the *d*-axis is aligned with the rotor flux. The absence of any physical sensor to obtain the peak rotor flux position leads to the necessity for design of an estimator to do the same. The fundamental equation governing the estimator model as discussed in Chapter 2 equation (2-11) and (2-13) is presented below in equation (3-20) to (3-25) and (8). The magnetizing rotor magnetizing

current i_{magr} is given by equation (3-21). Replacing equation (3-22) in equation(3-23) we get the equations governing the estimator model shown in equation (3-25). Figure 3-4 shows the MATLAB implementation of the estimator model.

$$\frac{d}{dt}\lambda_{rd} + \frac{\lambda_{rd}}{\tau_r} = \frac{L_m}{\tau_r} i_{sd} \quad (3\text{-}20)$$

$$i_{magr} = \frac{\lambda_{rd}}{L_m} \quad (3\text{-}21)$$

$$i_{magr} = i_{magr} + \frac{T_s(i_{sd} - i_{magr})}{\tau_r} \quad (3\text{-}22)$$

$$\omega_{dA} = \frac{i_{sq}}{\tau_r i_{magr}} \quad (3\text{-}23)$$

$$\omega_{da} = \omega_{mech} * (polepairs) + \omega_{dA} \quad (3\text{-}24)$$

$$\theta_{da} = \theta_{da} + \omega_{da} T_s \quad (3\text{-}25)$$

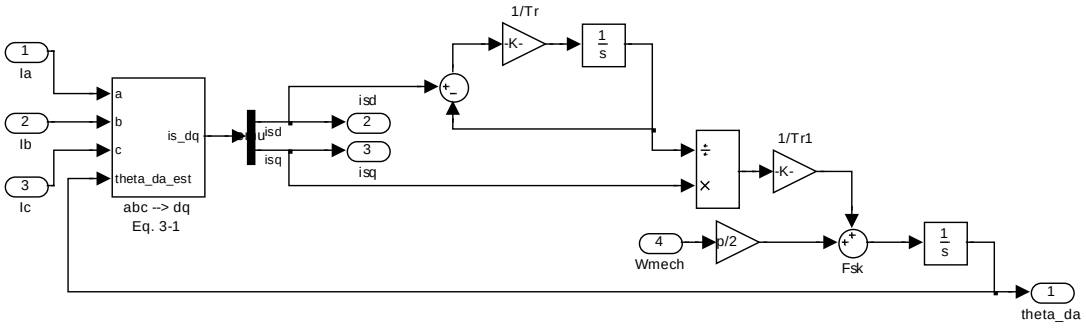

Figure 3-4 IM Estimator model block diagram

3.3.4 *dq* to *abc* model

The *dq* to *abc* model converts the control parameters represented in two axis system to the three axis system. This back transformation is necessary to convert the stator *dq* voltages to *abc*

voltages to be applied to the IM. The mathematical basis for this transformation has been discussed in Chapter 1 and the MATLAB representation of the same is shown in Figure 3-5.

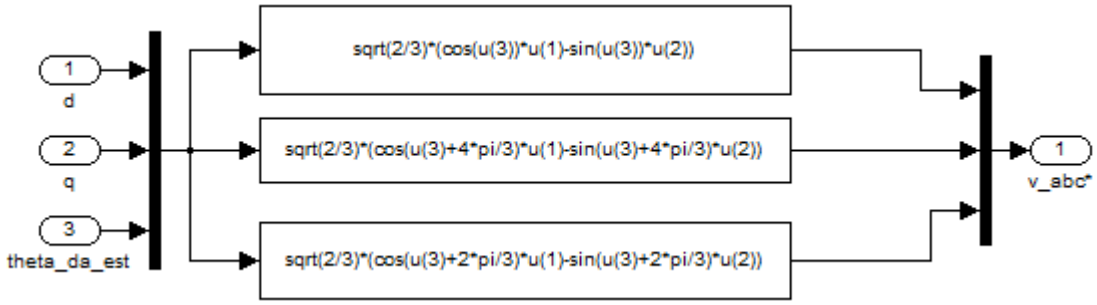

Figure 3-5 abc to dq transformation block diagram

3.3.5 Load model

The load is modeled as a frictional load as given in equation (3-26) where K_{fric} is the coefficient of friction. Figure 3-6shows the MATLAB implementation of the frictional load torque. In many applications the load is a linear function of speed and hence modeled as below.

$$T_{fl} = K_{fric}\omega_m \qquad (3\text{-}26)$$

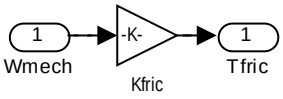

Figure 3-6 Friction model block diagram

3.3.6 Controller model introduction

As already mentioned in Chapter 2, the *d*-axis control is responsible for maintaining the rotor flux at its rated value and the q-axis control is responsible for controlling the torque. Both these forms of control can be achieved by using PI controllers since the signals in dq reference frame is typically dc. The design of PI controller has been discussed in Chapter 4 at length. Although PI

controllers are most popularly used in the industry, it presents a lot of design challenges. As an alternative to the PI controller, an observer based controller is introduced and designed in chapter 4.

3.4 Conclusion

In this chapter we looked we set the basic framework for simulation studies which were carried out to verify controller performance. The first section gave a broad overview of various subsystems that constituted vector control of IM followed by a mathematical model discussing each component. This provides an in-depth understanding into the various signal flows of the control system. The speed, current and flux controller need detailed discussion which has been discussed in Chapter 4. Since this chapter provides a thorough analysis of all the equations that make up the various subsystems along with their MATLAB models, it is a thorough rendering for anybody looking to learn vector control of IM. The following chapter talks about PI controller design for speed, current and flux controller. The Observer based controller, a relative newer form of control has been introduced as an alternative to PI based control. A simple comparative study between the PI based controller and Observer based controller.

Chapter 4

Controller Design

4.1 Introduction

From our discussion in the previous chapters we know that indirect vector control of induction motor can be achieved by controlling the rotor flux vector along the d-axis and the torque in the machine along the q-axis.

In the *d*-axis control the flux in the machine is maintained at its rated value by controlling the *d*-axis current, i_{sd}, at a predetermined reference value. i_{sd} current control is achieved by designing a PI controller that transforms the error in the stator d-axis current error to an appropriate stator d-axis voltage, v_{sd}. The steps used in the design of the PI controller are outlined in section 4.2.

The q-axis loop is responsible for providing the necessary torque to the machine thereby driving the IM to the required speed. For applications where speed control is desired, the speed error is transformed into reference current which in turn is transformed into the necessary voltage to drive the machine to the required speed. The PI controller design that transforms the stator *d*-axis current error to appropriate stator *q*-axis voltage v_{sd} is discussed in section 4.2.2.1. PI controller design for speed error transformation to reference i_{sq} is carried out in section 4.2.1. As a comparison to the PI controller, an observer based controller that transforms the speed error to reference i_{sq} is carried out in section 4.3. Finally, a simple comparative study between the PI based controller and observer based controller is carried out in section 4.4.

4.2 PI controller design

Over 90% of industrial control is of the simple proportional-integral-derivative (PID) type , which was proposed in 1922. The controller is designed empirically and does not require the mathematical model of the plant. The following section addresses the design of proportional-integral controllers based on a pre-decided cross over frequency and desired phase margin.

4.2.1 Design of PI speed controller

The speed controller is the outer loop along the q-axis and is responsible for transforming the speed error into an appropriate value of i_{sq}reference current which controls the torque in the machine. In the design of speed loop it is assumed that the d-axis current, i_{sd} is at its rated value ($i_{sd}{}^{*}$) and a direct relation between electromagnetic torque T_{em} and i_{sq} current can be derived as per equation (4-1) in steady state.

$$T_{em} = \frac{p}{2}\frac{{L_m}^2}{L_r} i_{sd}{}^{*} i_{sq} \qquad (4\text{-}1)$$

$$T_{em} = k i_{sq} \qquad (4\text{-}2)$$

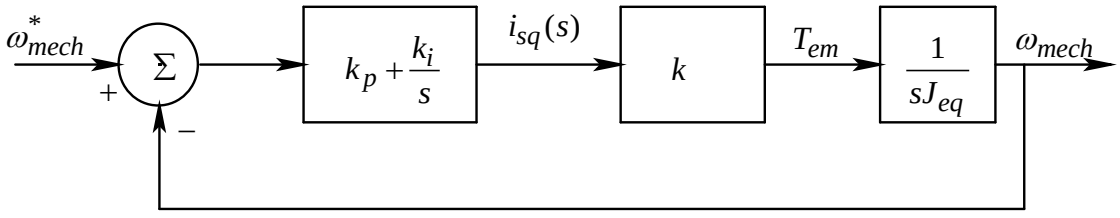

Figure 4-1 Design of q axis speed loop controller (Advanced Electric Drives by Ned Mohan, 2001: p.5-11)

The speed loop diagram is shown in Figure 4-1 where the proportional and integral constants are calculated based on a cross-over frequency of 100 Hz and phase margin of 60 degrees. This leads to conditions as per equation (4-3) and equation (4-4) and we get an empirical relation for the PI constants as per equation (4-5) and equation (4-6). We see that the PI constants are dependent on motor parameters inertia, pole pairs, magnetizing inductance and rotor leakage inductance. Thus, in order to have good control with the use of PI controllers it is important to have accurate measures of these motor parameters.

$$\left|\left(k_p + \frac{k_i}{s}\right)(k)\left(\frac{1}{sJ_{eq}}\right)\right| = 1 \quad (4\text{-}3)$$

$$\left(k_p + \frac{\widehat{k_i}}{s}\right)(k)\left(\frac{1}{sJ_{eq}}\right) = (180 - PM)^\circ \quad (4\text{-}4)$$

$$k_i = {\omega_c^2 J_{eq}}\Big/{(k\sqrt{1 + tan(PM)^2})} \quad (4\text{-}5)$$

$$k_p = \frac{k_i tan(PM)}{\omega_c} \quad (4\text{-}6)$$

Figure 4-2 is a bode plot of the open loop plant of the speed loop with and without the PI controller. We see from the bode plot that the open loop plant (G) with the PI controller (K) have a cross-over frequency of 100 Hz and phase margin of 60 degrees as per our design. We see how the PI controller improves performance of the system by giving better reference tracking at small frequencies and noise rejection at high frequencies. We know that for good reference tracking at low frequencies, we want the $|GK| > 1$ and for noise rejection at high frequencies we want$|GK| < 1$. In Figure 4-2 we see that the open loop plant with the controller has higher gain at low frequencies and thus provides better reference tracking capabilities. At high frequency's

where noise is prevalent the gain of the plant with PI controller rolls off to provide noise rejecting capabilities.

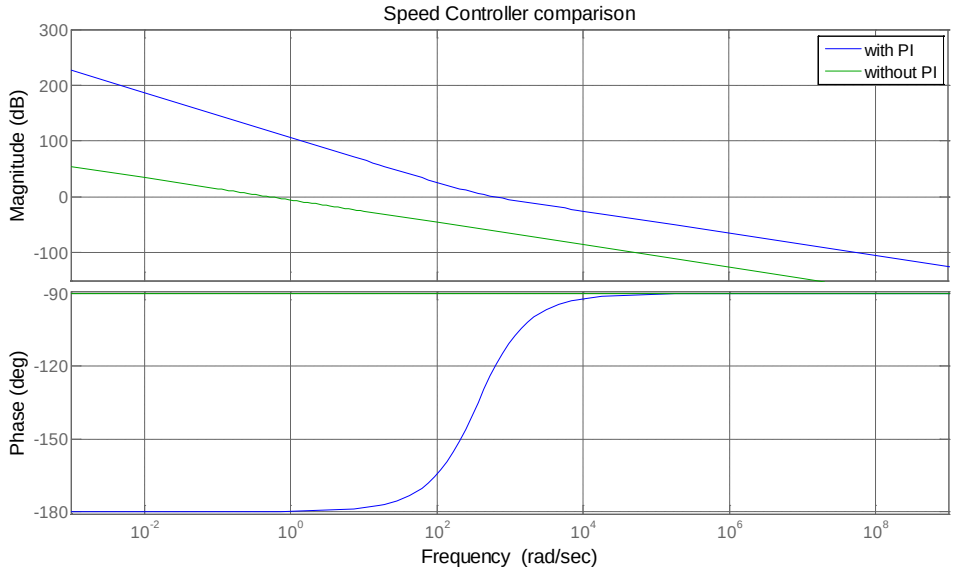

Figure 4-2 Influence of speed PI controller on performance of speed loop controller

4.2.2 Design of PI Current and Flux controller

The current and the flux loop design are done using the same procedure and similar equations govern their operation. Both these loops transform their respective axis dq-axis currents to appropriate dq-axis voltages to be fed into the IM.

4.2.2.1 Flux controller

We know from Chapter 3 equation (3-20)that rotor d-axis flux λ_{rd} can be controlled by the stator d-axis current i_{sd}. Hence, we can operate the machine at the rated magnetizing flux λ_{rd}^{*} by controlling stator d-axis current to be maintained at i_{sd}^{*}. The relation between λ_{rd}^{*} and i_{sd}^{*} is derived in Chapter 2 equation (2-11). Therefore, the reference to the stator d-axis current is i_{sd}^{*}

and a PI controller governs the conversion of the error in the estimated i_{sd} current from i_{sd}^{*} to the appropriate stator d-axis voltage v_{sd} .

The relation between v_{sd} and i_{sd} is shown in equation (4-7). We notice two additional terms dependent on rotor d-axis flux λ_{rd} and the stator q-axis current i_{sq} which can be seen as a cross coupling within the loops. We can treat these terms as disturbances and design our q-axis current loop using the relation in equation (4-8).

$$v_{sd} = R_s i_{sd} + \sigma L_s \frac{d}{dt} i_{sd} + \frac{L_m}{L_r} \frac{d}{dt} \lambda_{rd} - \omega_d \sigma L_s i_{sq} \quad (4\text{-}7)$$

$$v_{sd}{}' = R_s i_{sd} + \sigma L_s \frac{d}{dt} i_{sd} \quad (4\text{-}8)$$

$$Where\ \sigma = 1 - \frac{L_m^2}{L_s L_r} \quad (4\text{-}9)$$

The flux loop diagram is shown in Figure 4-3 where the proportional and integral constants are calculated based on a cross-over frequency of 1000 Hz and phase margin of 60 degrees. Here we choose the crossover frequency of the current loop to be ten times more than the crossover frequency of the speed loop since it is desirable for us to be able to provide fast changing current for superior transient performance. The assumed cross-over frequency and phase margin leads to equation (4-10) and equation (4-11) which leads to proportional and integral gains as per equation (4-12) and equation (4-13).

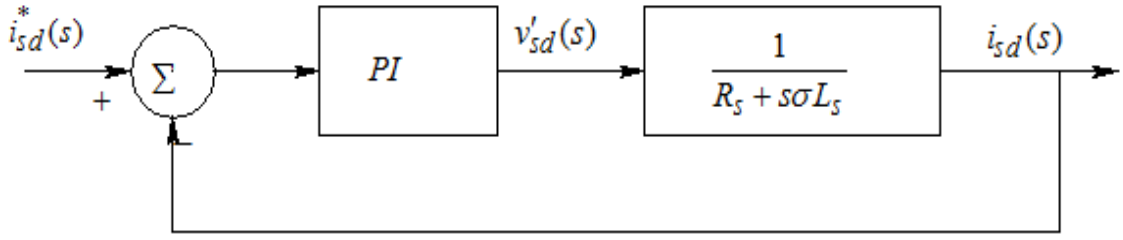

Figure 4-3 Design of dq current loop controller (Advanced Electric Drives by Ned Mohan, 2001: p.5-15)

$$\left|\left(k_p + \frac{k_i}{s}\right)\left(\frac{1}{R_s + s\sigma L_s}\right)\right| = 1 \quad (4\text{-}10)$$

$$\widehat{\left(k_p + \frac{k_i}{s}\right)\left(\frac{1}{R_s + s\sigma L_s}\right)} = (180 - PM)^{\circ} \quad (4\text{-}11)$$

$$k_i = \sqrt{\frac{R_s^2 + (\omega_{ci} L_s \sigma)^2}{tan(PM - \frac{\pi}{2} + tan^{-1}(\frac{\omega_{ci} L_s \sigma}{R_s}))^2 + 1}} \quad (4\text{-}12)$$

$$k_p = \left(\frac{tan\left(PM - \frac{\pi}{2} + tan^{-1}\left(\frac{\omega_{ci} L_s \sigma}{R_s}\right)\right)}{\omega_{ci}}\right) \sqrt{\frac{R_s^2 + (\omega_{ci} L_s \sigma)^2}{tan(PM - \frac{\pi}{2} + tan^{-1}(\frac{\omega_{ci} L_s \sigma}{R_s}))^2 + 1}} \quad (4\text{-}13)$$

4.2.2.2 Current controller

The current loop is the inner loop along the q-axis and is responsible for transforming the stator q-axis current error to appropriate stator$q$-axis voltage (v_{sq}). The relation between v_{sq} and i_{sq} is shown in equation (4-14). In equation (4-14) we notice two additional terms dependent on rotor d-axis fluxλ_{rd} and the stator d-axis current i_{sd}. We can treat these terms as disturbances and design our q-axis current loop using the relation in equation (4-15).The design of the flux loop is

$$v_{sq} = R_s i_{sd} + \sigma L_s \frac{d}{dt} i_{sq} + \omega_d \frac{L_m}{L_r} \lambda_{rd} + \omega_d \sigma L_s i_{sq} \quad (4\text{-}14)$$

$$v_{sq}{}' = R_s i_{sq} + \sigma L_s \frac{d}{dt} i_{sq} \quad (4\text{-}15)$$

$$Where\ \sigma = 1 - \frac{L_m^2}{L_s L_r} \quad (4\text{-}16)$$

The design of proportional and integral constants for *q*-axis current loop is similar to the design for the flux loop. Following the exact same procedure gives us the same values of proportional and integral gains as for the flux loop.

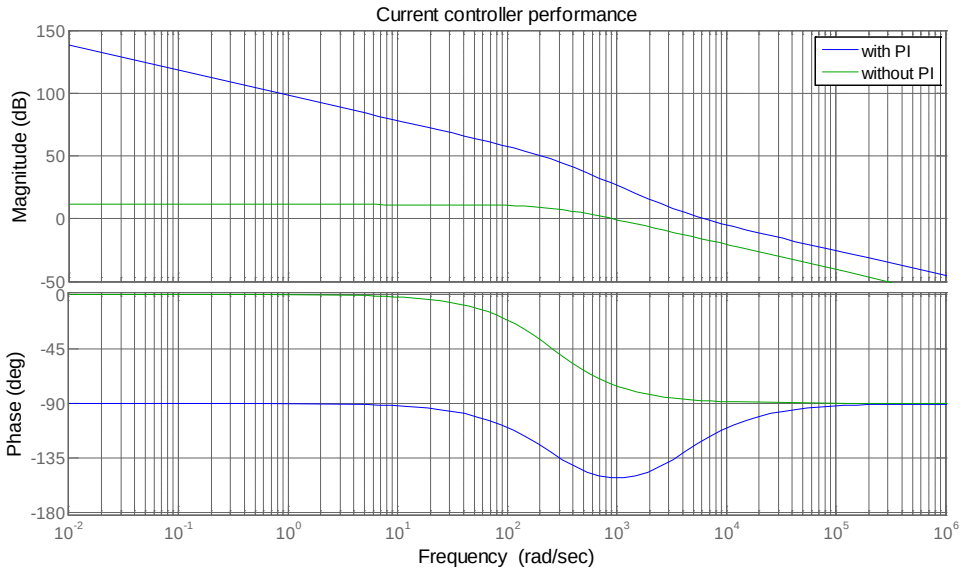

Figure 4-4 Influence of current PI controller on performance of current loop

Figure 4-4 is a Bode plot of the open loop plant of the current loop with and without the PI controller. We see from the bode plot that the open loop plant (G) with the PI controller (K) have a cross-over frequency of 1000 Hz and phase margin of 60 degrees as per our design. Following our discussion on the controller in the speed loop, we see that the open loop plant with the

controller has higher gain at low frequencies and rolls off rapidly at low frequencies thus providing better reference tracking and noise rejecting capabilities.

4.3 Observer based controller design

4.3.1 Overview

PID controllers are the most commonly used controllers in the industry for a long time now. But, the ever increasing demands for ease of tuning, robustness and efficiency have forced control engineers to look beyond this controller for and other approaches. Figure 4-5 represents a block diagram representation of the observer based controller. It consists of the external observer which takes the output speed and the input to the plant as the input and computes the various states which are used as inputs in the forward loop. A proportional controller is used to model the system as a integrator as shown in the discussions below. In motor control applications such as this, k_t is the torque constant of the machine. In the following discussion the observer based controller design for vector control is discussed based on the research carried out in (9).

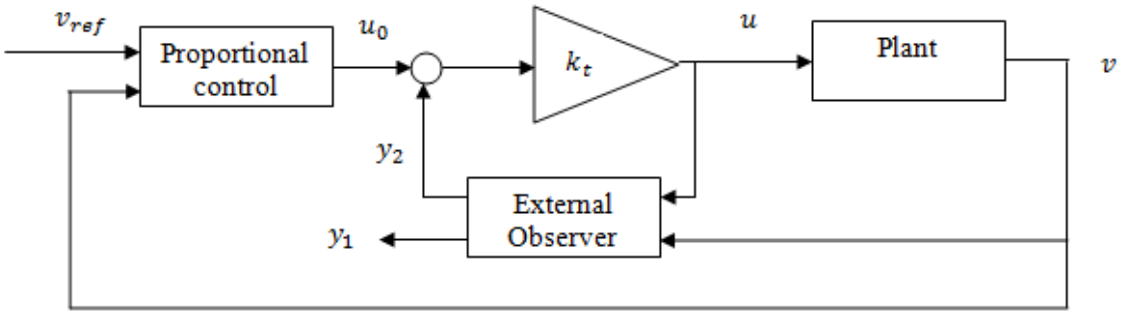

Figure 4-5 Block diagram overview of observer based controller

4.3.2 Mathematical model

In a typical application using a motor as the application, the equation of motion can be described as:

$$\dot{v} = f(t, v, d) + bu \quad (4\text{-}17)$$

Where v is velocity which is the output of the system and u is the input motor current, b is the torque constant, and d represents the external disturbance such as vibrations and friction. In the above equation, $f(*)$ encapsulates the dynamic equation of the IM along with other factors such as system inertia, friction. Equation (4-17) can be written as

$$\dot{v} = f(t, v, d) + \frac{k_t}{J} i \quad (4\text{-}18)$$

Let us write out the state space equation of this generic model of a system described in equation (4-18) as shown below in equations (4-19) and (4-20).

$$X_1 = v \; and \; \dot{X}_1 = X_2 + \frac{k_t}{J} i \quad (4\text{-}19)$$

$$X_2 = f and \; \dot{X}_2 = \dot{f}$$

$$\begin{bmatrix} \dot{X}_1 \\ \dot{X}_2 \end{bmatrix} = \begin{bmatrix} 0 & 1 \\ 0 & 0 \end{bmatrix} \begin{bmatrix} X_1 \\ X_2 \end{bmatrix} + \begin{bmatrix} \frac{k_t}{J} \\ 0 \end{bmatrix} [i] + \begin{bmatrix} 0 \\ 1 \end{bmatrix} [\dot{f}] \quad (4\text{-}20)$$

$$[v] = [1 \quad 0] \begin{bmatrix} X_1 \\ X_2 \end{bmatrix}$$

$$A = \begin{bmatrix} 0 & 1 \\ 0 & 0 \end{bmatrix} B = \begin{bmatrix} \frac{k_t}{J} \\ 0 \end{bmatrix} C = [1 \quad 0] E = \begin{bmatrix} 0 \\ 1 \end{bmatrix}$$

The central idea behind this concept is to model everything unknown, uncertain about the system as a part of the extra state X_2 and by use of an extended state observer estimate X_2 to be able to compensate for all the unknowns about the system. This is especially significant in motor controls because it is very common for a motor controls engineer to have inaccurate measure of the motor

parameters which adds to the uncertainty in the system. For motor control applications where disturbance is a common occurrence, this controller is of significance as this estimate the disturbance in the system as part of X_2 and compensates for it in real time.

The state observer for the above system can be described as per equation (4-21). With the observer gain $L = [l1 \quad l2]^T$ selected appropriately, it provides the estimate of the state $Z_1 = X_1$ and $Z_2 = X_2$.

$$\dot{Z} = AZ + Bi + L(y_1 - v) \tag{4-21}$$

$$y = CZ$$

The estimator gain L is tuned by using pole-placement method of $A - LC$ matrix of the observer. In this design, both the poles are positioned at a frequency ω_0 in the left half of the *s*-plane. The observer gains are parameterized as per equation (4-22)and observer state space representation are shown in equation (4-23).

$$L = [2\omega_0 \quad \omega_0^2]^T \tag{4-22}$$

$$\begin{bmatrix} \dot{Z}_1 \\ \dot{Z}_2 \end{bmatrix} = \begin{bmatrix} -2\omega_0 & 1 \\ -\omega_0^2 & 0 \end{bmatrix} \begin{bmatrix} Z_1 \\ Z_2 \end{bmatrix} + \begin{bmatrix} \frac{k_t}{J} & 2\omega_0 \\ 0 & \omega_0^2 \end{bmatrix} \begin{bmatrix} i \\ v \end{bmatrix} \tag{4-23}$$

$$\begin{bmatrix} y_1 \\ y_2 \end{bmatrix} = \begin{bmatrix} 1 & 0 \\ 0 & 1 \end{bmatrix} \begin{bmatrix} Z_1 \\ Z_2 \end{bmatrix}$$

For a well tuned observer, the observer state Z_2 will closely track $X_2 = f$. Now consider an input *u* in accordance with equation (4-24). This reduces equation (4-17) as per equation(4-25) which is a model of an integrator and can be easily controlled using a proportional controller. Equation (4-26) is a model of the proportional controller which transforms the speed error to u_0 which results in $k_p = \omega_c$. v_{ref} is the reference velocity set-point.

$$i = \frac{-y_2 + i_0}{\frac{k_t}{J}} \quad (4\text{-}24)$$

$$\dot{v} = i_0 \quad (4\text{-}25)$$

$$\dot{v} = k_p(v_{ref} - v) + \dot{v_{ref}} \quad (4\text{-}26)$$

4.4 Comparative study between PI and Observer based controllers

Below is a simple simulation study that compares the PI based controller and Observer based controller. Since the Observer based controller has been implemented only in the speed loop, it is compared to the speed loop PI controller.

Figure 4-6 Reference tracking and disturbance rejection for observer based controller

The PI controller used is the same as the one used for simulation studies of PI controller based Vector control analysis and the observer based controller used is the same as for Observer based Vector control. To compare the performance of the controller, a reference tracking test is carried out with disturbance injection. Figure 4-6 shows the performance of the observer based controller to a reference command of 1 unit and disturbance injection of 0.5 units at 3 seconds.

We notice that the observer based controller does a good job of being able to track the reference and reject disturbance with very little overshoot. Figure 4-7 shows the performance of PI based controller to the same input conditions. We notice that the PI based controller has a much longer rise time and bigger overshoot.

It is important to understand that the performance of the PI controller does not reflect its capabilities but the extent to which it has been tuned for the application. As mentioned in Chapter 3, much of the motor parameters were unknown and this is reflected in poor performance of the PI controller. Since the Observer based controller does not depend on system parameters and treats all uncertainties as a single state, we see that it does a better job. Table 4-1 compares the PI and Observer based controller against performance metrics.

Table 4-1 Comparison of PI and observer based controller against performance metrics

Performance metric	PI controller	Observer controller
Rise time (sec.)	0.12	.0004
Disturbance Overshoot (%)	3335	10.7
Settling time (sec.)	1.05	.02
Steady state error (%)	0	0

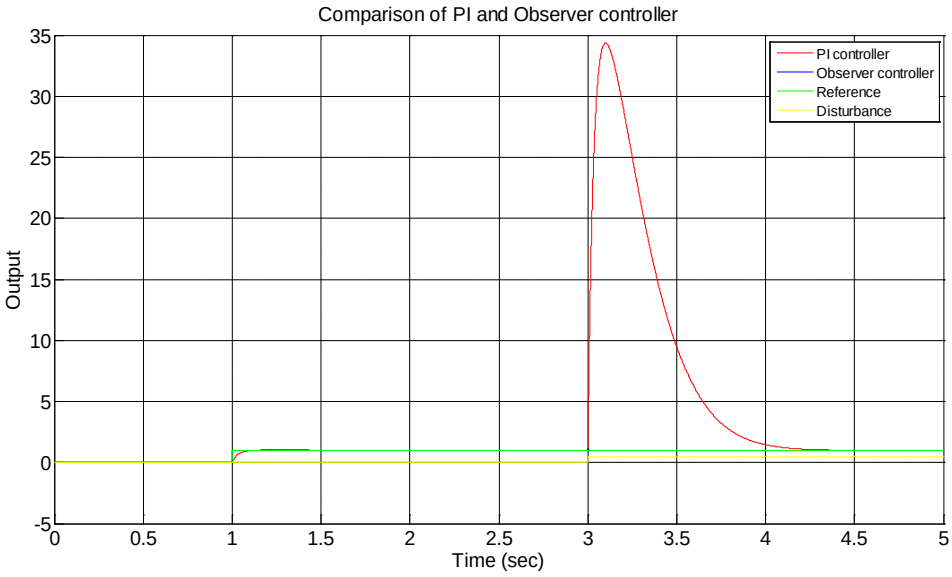

Figure 4-7 Comparison of PI and observer based controller to speed reference tracking and disturbance rejection

4.5 Conclusion

In this chapter we discussed the various aspects about design of controller for IM. We discussed about two different kinds of controller – PI based controller and Observer based controller. We discussed the design of PI based controller for speed current and flux loop and the various interdependencies and considerations between the inner and outer loop. It is shown how design of PI controller is heavily dependent on system parameters and questions the validity of the design for systems whose motor parameters are inaccurate. An analysis into each of the controller was carried out by comparing it to a base line condition. As an alternative to the PI controller, an Observer based controller was introduced as an attempt to tackle the challenges posed by the PI based controller. A simple comparative study between the PI based controller and Observer based controller was carried to compare their performances. The performance of the Observer based controller was found to be better and was tested in vector control application and results are provided in Chapter 5.

Chapter 5

Simulation and Hardware results

5.1 Introduction

Induction motors have been the area of research focus due to its ruggedness and longevity. Advances in power electronics have enabled implementation of new control topologies. Numerical simulation tools are an important tool to verify the operation of new controllers. In this study, MATLAB/ Simulink simulation software, a mathematical tool developed by The Mathworks, has been used to verify the controller design. Vector Control of IM using PI controller and observer based controller has been simulated and the results are presented in section 5.2.2. Hardware implementation of the same was carried out and the results have been presented in section 5.3.2.

5.2 Design and simulation results

5.2.1 Design Results

Following the design procedure described in Chapter 3, section3.2 the motor parameters were determined and the results are in Table 5-1. Simulation results for vector control of IM have been presented using both PI based controller and Observer based controller. The PI controller design was carried out using the procedure outlined in Chapter 4 section 4.2 and the results are presented in Table 5-2. Following the design discussion on the Observer based controller, the design parameters used are listed in Table 5-3. It can be seen that the Observer based controller relies

only on two parameters compared to the PI based controller and is easier to tune than the PI based controller.

Table 5-1 Motor electrical parameters

Stator resistance (R_s)	0.275 Ω
Stator leakage inductance (L_{ls})	0.0012 Henry
Magnetizing inductance(L_m)	0.0053 Henry
Rotor leakage inductance referred to stator (L_{lr})	0.0018 Henry
Rotor resistance referred to stator (R_r')	0.2729 Ω

Table 5-2 PI controller design for speed and current loop

Proportional gain speed loop	0.0176
Integral gain speed loop	$3.7516e^5$
Proportional gain current loop	0.0274
Integral gain current loop	$2.2357e^4$
Proportional gain flux loop	0.0274
Integral gain flux loop	$2.2357e^4$

Table 5-3 Observer based controller design

Observer bandwidth	6 radians/sec
P controller bandwidth	60 radians/sec

5.2.2 Simulation results:

The simulation results presented below represent the performance of the controllers to speed reference tracking, speed controller response, current controller response, flux controller response, the motor phase voltage and current waveforms.

Table 5-4 PI based vector control simulation results

PI based Vector Control
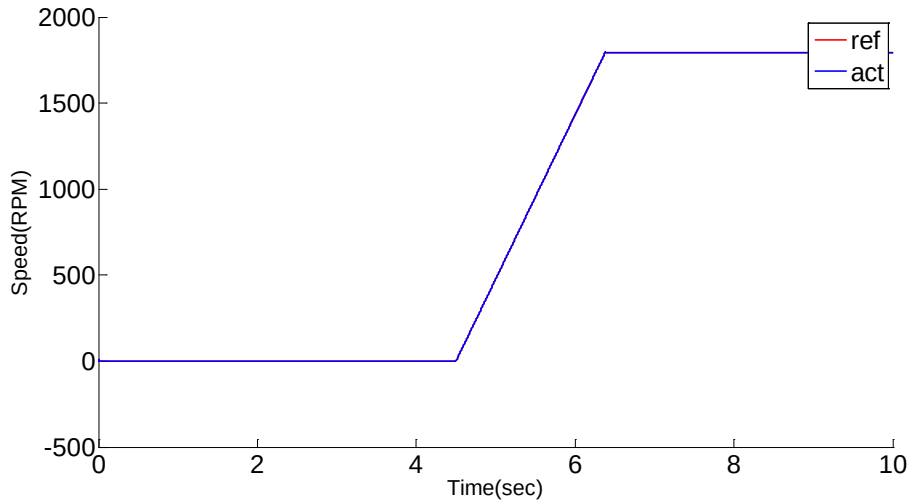
Figure 5-1 Simulation of speed reference tracking for PI controller
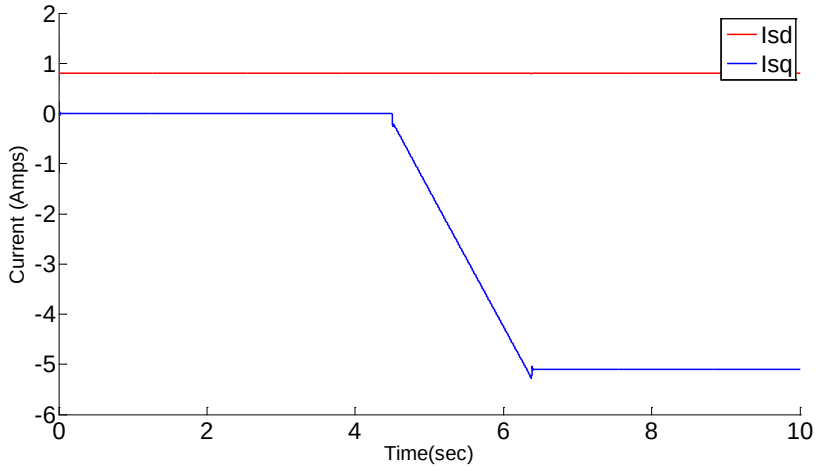

Figure 5-2 Simulation of stator dq currents for PI based controller

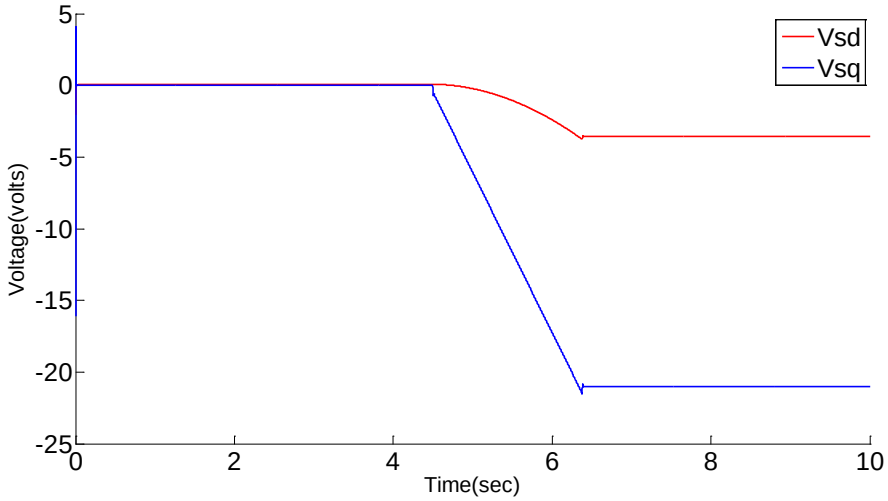

Figure 5-3 Simulation of stator dq voltage for PI based controller

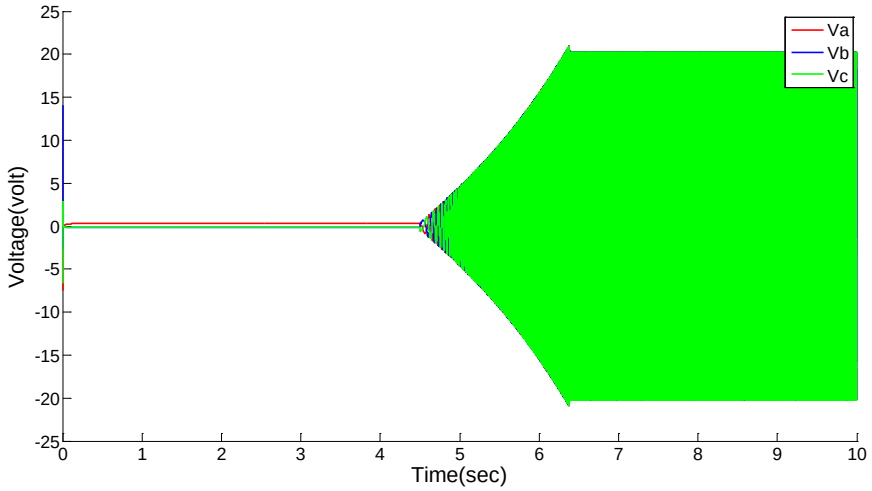

Figure 5-4 Simulation of phase voltage waveform for PI based controller

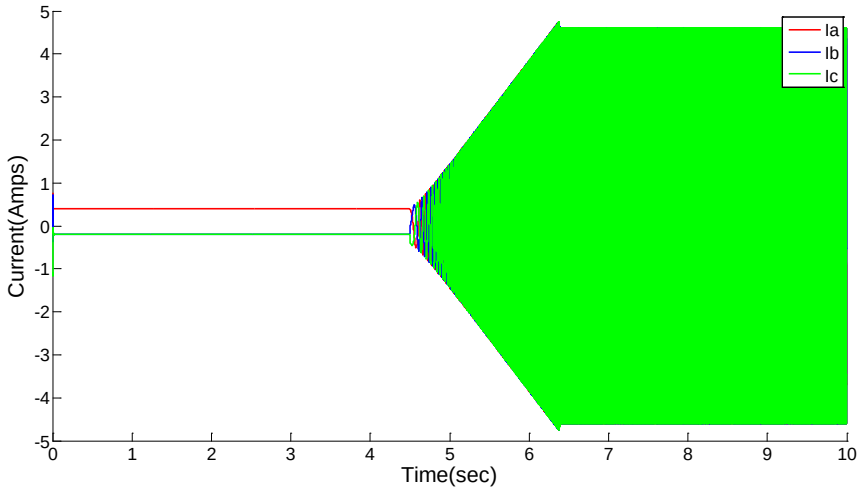

Figure 5-5 Simulation of phase current waveform for PI based controller

Table 5-5 Observer based vector control results

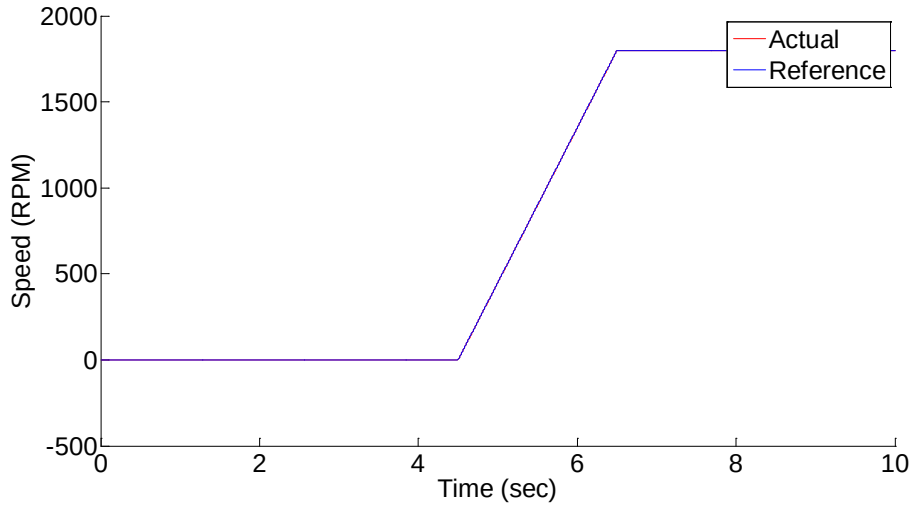

Figure 5-6 Simulation speed reference tracking for Observer based controller

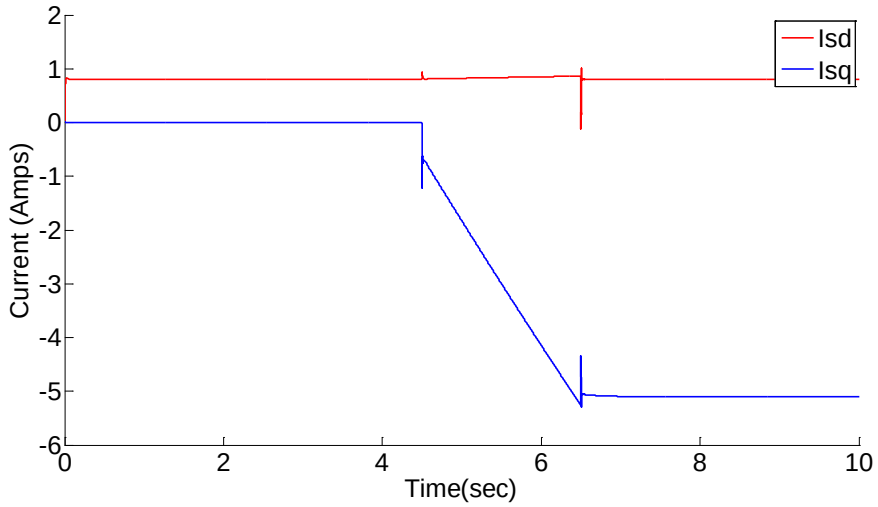

Figure 5-7 Simulation dq current for Observer based controller

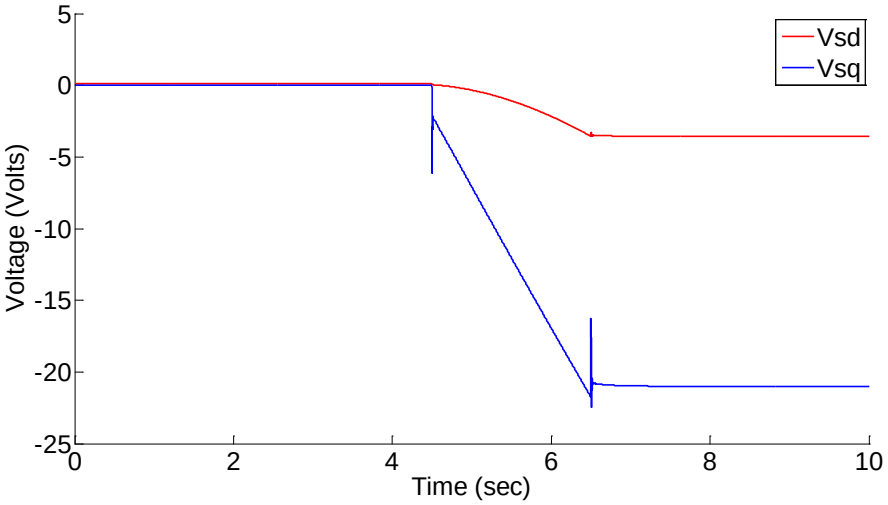

Figure 5-8 Simulation stator dq voltage for Observer based controller

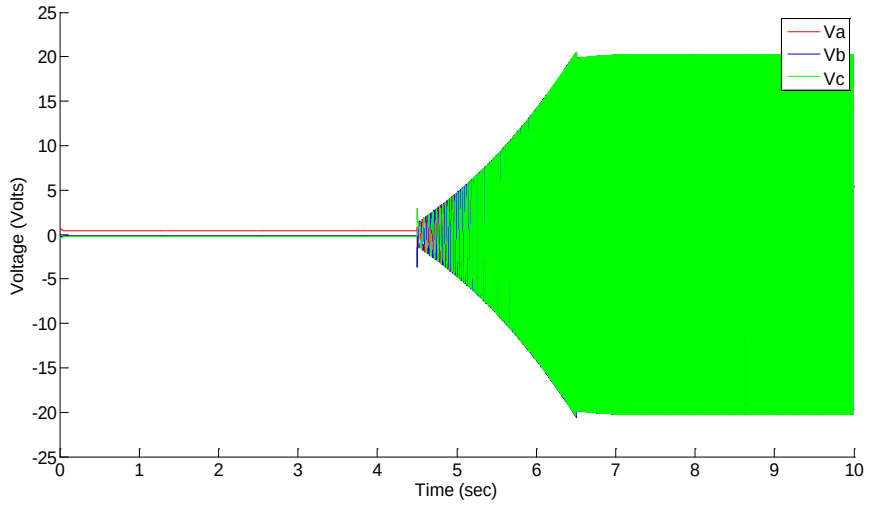

Figure 5-9 Simulation stator phase voltage for Observer based controller

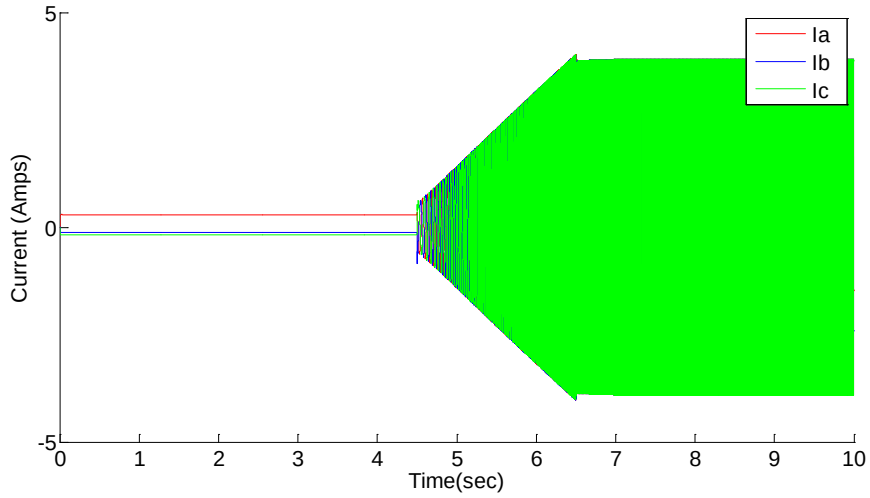

Figure 5-10 Simulation phase current for Observer based controller

5.2.2.1 Speed reference tracking

In the above simulation results, the speed reference command is given at time 4.3 seconds. Figure 5-1 and Figure 5-6 shows the speed reference tracking results for the PI based controller and the observer based controller. We see that both these controllers track the reference speed with no

steady state error. It was also observed that the observer based controller does a better job than PI based controller when it comes to overshoot and rise time. This was also observed in Chapter 4 section 4.4.

5.2.2.2 Stator *dq*-axis current

Figure 5-2 and Figure 5-7 shows the stator *dq*-axis current for the PI based controller and observer based controller. We see that the PI based controller traces a smoother trajectory in comparison to the observer based controller. This is because the PI based controller was tuned to respond to this input signal where as the observer based controller has its inherent advantages. We see that the i_{sq} current increases as the speed increases. This is because, the load torque is modeled to increase in proportion to the speed and this results in an increase in the stator *q*-axis current until the reference speed steadies.

5.2.2.3 Stator *dq*-axis voltage

Figure 5-3 and Figure 5-8 shows the stator *dq*-axis voltages for the PI based controller and observer based controller. We see that the v_{sq}voltage increases in magnitude as long as the i_{sq} current increases in magnitude. Interestingly, we notice that v_{sd} increases while the speed ramps. One would expect v_{sd} to be a constant to ensure constant rotor flux linkage. However, we should remember that there are cross coupling terms between the *d* and *q*as discussed in equation (4-14) and equation (4-15). The effect of *q*-axis dynamics piles on the *d*-axis voltage to generate a ramp like voltage along the *d*-axis. This is undesirable.

5.2.2.4 Stator Voltage and Current

Figure 5-4, Figure 5-5 and Figure 5-9, Figure 5-10 show the stator voltage and current waveforms for the PI and Observer based controller respectively. We notice that the stator phase voltage waveform has its peak at 20 V and current at 4.1 A.

5.3 Hardware setup and results

5.3.1 Hardware setup

The above simulation results have been verified using a hardware prototype. The hardware prototype consists of a University of Minnesota propriety 3-inverter power electronics board. The 3-inverter board consists of three inverter modules used for driving a motor and an active load at the same time. This board can also be used for doubly fed induction generator (DFIG) applications where two inverter modules are used for the DFIG and one inverter module for the active load. The board is rated for input of 42 V dc supply and 4 Amperes of continuous current. The IRAM 136-3063B 30A 600V integrated power hybrid IC motor driver is used in the inverter modules. The driver provides inbuilt over voltage and over current protection and the board has hardware based break before make circuitry for the inverter.

The gating sequence for the inverter module is obtained from dSpace through a D-sub interface. The DS1104 controller board generates the digital control signal used for switching the inverter. The CP1004 I/O board is an interface board between the DS1104 controller and 3-inverter board used to read the analog signals in the application and feed the results to the DS1104 board for control. MATLAB-Simulink real time workshop is used to build the control algorithms and this is programmed into the DS1104 board.

The IM under test name plate details is provided in Table 5-6and the DC motor load name plate details is presented inTable 5-7. The DC motor is run as an active load to model the frictional element discussed in Chapter 3 section 3.3.5. The DC motor is run in torque control such that it sets a reference torque based on the shaft speed of the IM. Although controller design of IM was carried out and the design was verified using the simulation results, the PI constants provided oscillatory performance during hardware implementation. Hence, a trial and error approach in

tuning the hardware PI constants was used and the results are presented in Table 5-8. The failure of the designed PI controller in hardware implementation can be attributed to inaccurate measure of the motor parameters.

Table 5-6 Induction motor name plate details

Rated power	120 W
Voltage	30 VAC
Maximum speed	4000 RPM
Rated Ampere	6 A
Frequency	60 Hz
Pole pairs	2
Inertia	.000225 Kg-m^2

Table 5-7 DC motor name plate details

Rated Voltage	40 V
Rated output power	180 Watts at 3500 RPM
No load speed	5000 RPM
Ke	9.5 V/KRPM
Kt	.081 Nm/A
Rotor Inertia	0.000007 Kg-m^2

Table 5-8 Hardware speed and current PI controller design

Proportional gain speed loop hardware	0.442
Integral gain speed loop hardware	6.39

Proportional gain current loop hardware	0.4368
Integral gain current loop hardware	109.2392
Proportional gain flux loop hardware	0.4368
Integral gain flux loop hardware	109.2392

5.3.2 Hardware results

The hardware results presented below match the simulation results presented in Chapter 5 section 5.2.2. The performance of the controller in the hardware implementation is shown below in the form of speed reference tracking, *dq*-current waveforms, *dq*-voltage waveforms, phase voltage and current waveform.

Table 5-9 Hardware results for PI based controller

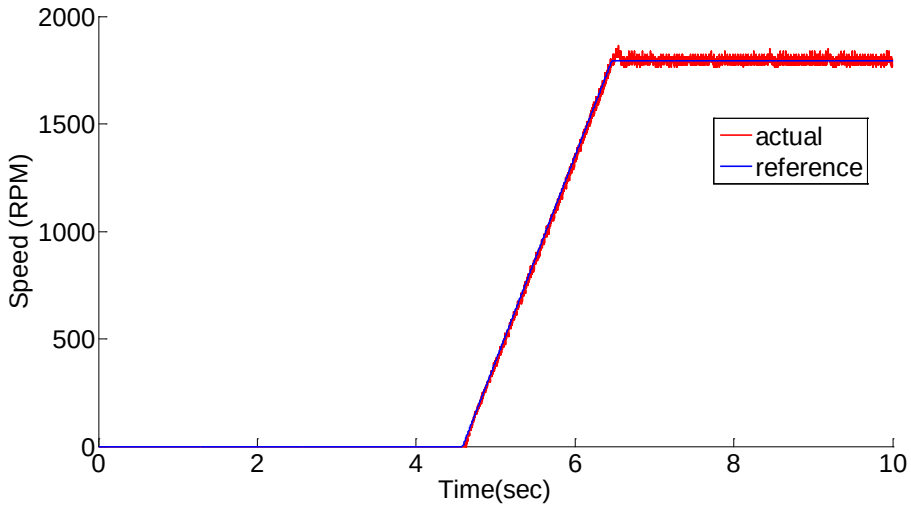

Figure 5-11 Hardware speed reference tracking for PI based controller response.

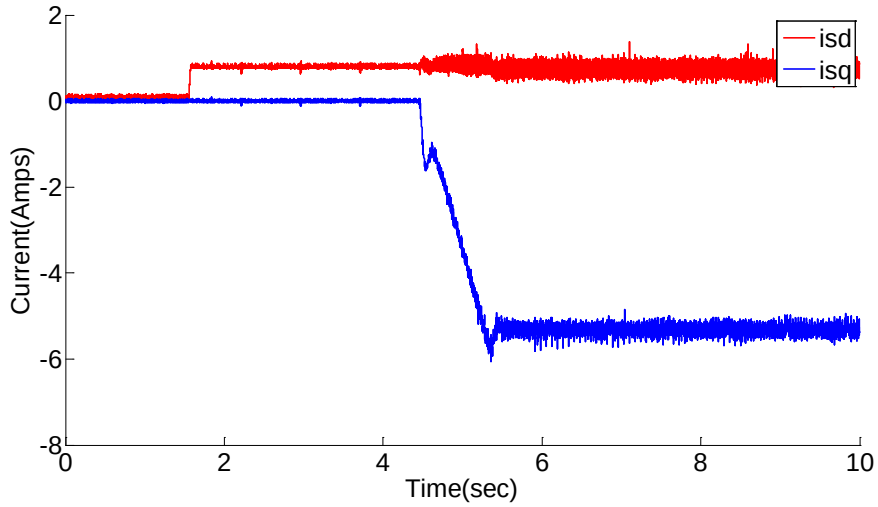

Figure 5-12 Hardware stator dq-axis current for PI controller response

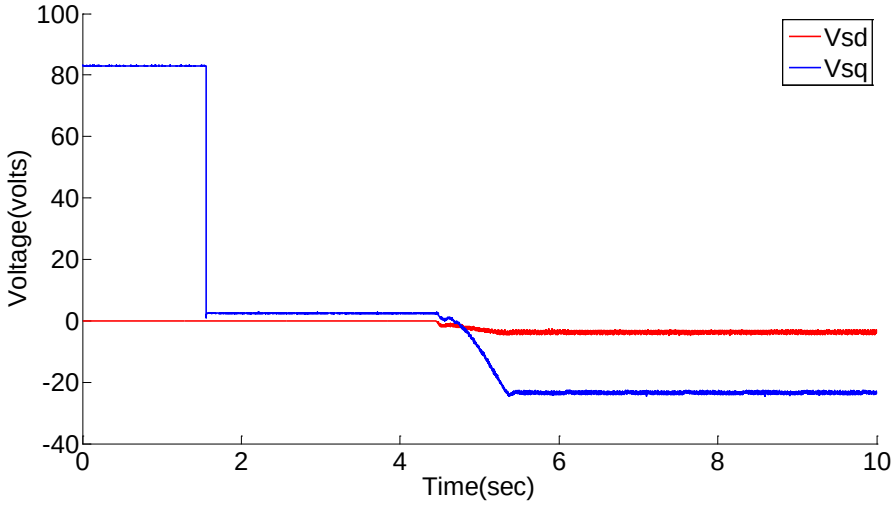

Figure 5-13 Hardware stator dq-axis voltage for PI controller response

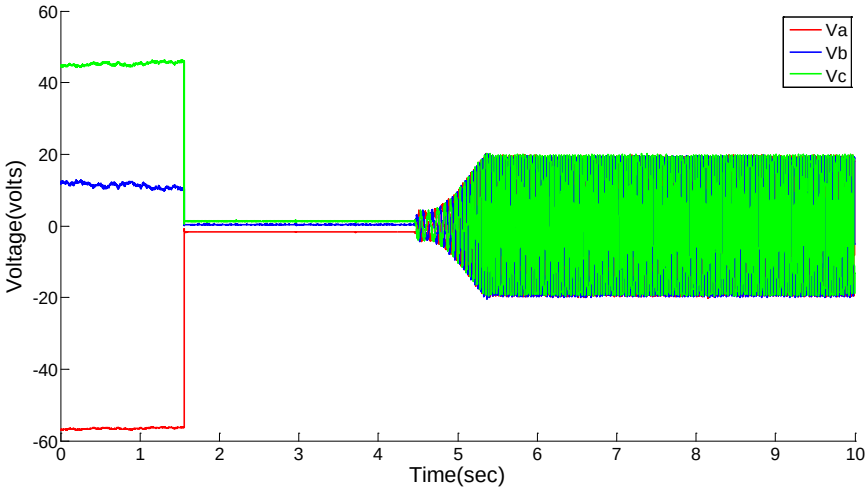

Figure 5-14 Hardware stator phase voltage for PI controller response

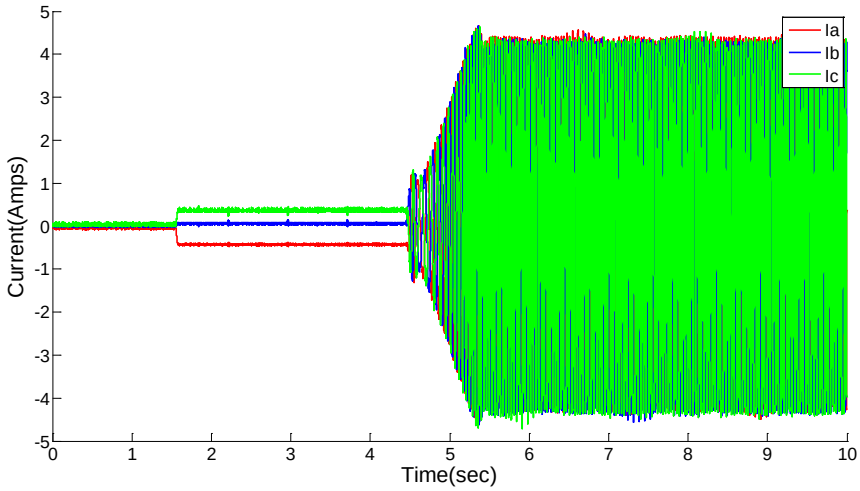

Figure 5-15 Hardware stator phase current for PI controller response

5.3.2.1 Speed reference tracking

Figure 5-11shows the IM speed response to the speed reference tracking. The speed reference command is given at 4.3 seconds and it can be seen that the motor tracks the reference speed comfortably.

5.3.2.2 Stator *dq*-axis current

Figure 5-12shows the IM stator *dq*-axis current. We see that prior to 4.3 seconds when the speed reference command is given; the stator *d*-axis current reaches its rated magnetizing value. This ensures that the motor is magnetized and to its rated value along the *d*-axis and is ready to obey torque command signals along the *q*-axis. The i_{sq} command is given at 4.3 seconds which results in increment of speed of the IM.

5.3.2.3 Stator *dq*-axis voltage

Figure 5-13shows the IM stator *dq*-axis voltage waveform. We see that the hardware results are in agreement with the results obtained through simulation.

5.3.2.4 Stator Voltage and Current waveforms

Figure 5-14and Figure 5-15 show the stator voltage and current waveforms for the hardware implementation of PI based controller. We notice that the stator phase voltage waveform has its peak at 20 V and current at 4.1 A. This performance is in agreement with the simulation results obtained earlier.

5.4 Conclusion

This chapter discusses the simulation and hardware results in detail. In addition to the results, it also discussed the tools that were used to obtain these results and all the hardware setup that was used to conduct the testing. Simulation and hardware results for PI based and Observer based vector control were presented. A comparative study into controller performance was carried out and results were put in perspective. It was seen that a well tuned PI controller performed better than the Observer based controller. It was seen that the Observer based controller was less complex than (5) the PI based controller and provided reasonable control performance.

5.5 Scope for future research

Motor controls are a field of study that encompasses three independent subjects: Electrical machines, Control systems and embedded systems. This presents many areas for further research with different focuses. Suggestions are given below keeping in mind the foundation that has been set in this thesis project.

- Equation (4-7)and equation (4-14) discusses the cross coupling terms that are present in the design of the current and flux controllers, the influence of which is seen in Figure 5-11. To overcome this cross-coupling between the *d* and *q* axis, a feed-forward term can be implemented.
- Chapter 3 discussed the method used to estimate the motor parameters and the inaccuracies associated with these methods. A more accurate method such as parameter estimation using regulators of drive system discussed in can be used to determine the motor parameters.
- The advantages of the observer based controller were discussed in Chapter 4 section 4.4. A more rigorous study of the observer based controller can be carried out followed by a practical implementation. This has a scope to open up a completely new approach to motor controls.
- Mechanical parameters such as motor Inertia and Friction can be determined experimentally for greater accuracy.
- A sensorless vector control strategy implementation.

Bibliography

1. **Mohan, Ned.** *Electric Drives An Integrative Approach.* Minneapolis : MNPERE, 2003.

2. *Comparison of Scalar and Vector Control strategies of Induction motor.* **G. Kohlrusz, D. Fodor.** 265-270, Veszprem : Hungarian Journal of Industrial Chemistry, 2011, Vol. 39 (2).

3. **Mohan, Ned.** *Advanced Electric Drives Analysis Control and Modelling.* Minneapolis : MNPERE, 2001.

4. **HOLTZ, JOACHIM.** *Sensorless Control of Induction Motor Drives.* Wuppertal : IEEE, VOL. 90, NO. 8, 2002.

5. *A simple Induction Motor Parameter Estimation Method for Vector Control.* **Wook-Jin Lee, Young-Doo Yoon, Seung-Ki Sul, Yoon-Young Choi, Young-Seok Shim.** 2007. Power Electronics and Applications .

6. *The effect of parameter variations on the performance of indirect vector controlled induction motor drive.* **A Shiri, A Vahedi, A Shoulaie.** Montreal : s.n., 2006.

7. **Minnesota, University of.** Electric Machines and Drives. *Consortium of Universities for Sustainable power.* [Online] http://cusp.umn.edu/.

8. **Dave Ross, John Theys, Steve Bowling.** Using the dsPIC30F for Vector Control of ACIM. *Microchip Technologies.* [Online] 2007. http://www.microchip.com/stellent/idcplg?IdcService=SS_GET_PAGE&nodeId=1824&appnote=en533872.

9. *Active Disturbance Rejection Control: A Paradigm Shift in Feedback Control System Design.* **Gao, Zhiqiang.** Minneapolis : s.n., 2006. American Control Conference.

10. *Direct Space Vector Modulated Three Level Matrix Converter.* **Siddharth Raju, LakshmiNarayanan Srivatchan, Ned Mohan.** Long Beach : s.n., 2013. Applied Power Electronics Conference and Exposition.